J. Fluid Mech. (1991), *vol.* 236, *pp.* 415–444
Printed in Great Britain

The kinematics of stretching and alignment of material elements in general flow fields

By ELIOT DRESSELHAUS AND M. TABOR
Division of Applied Mathematics, Department of Applied Physics, Columbia University, New York, NY 10027, USA

(Received 2 October 1990 and in revised form 19 August 1991)

A rigorous, kinematic description of the stretching and alignment of infinitesimal material elements in general flow fields is presented. An evolution equation is derived, in the Lagrangian frame, for the alignment angles between a material element and the principal axes of strain. The equation identifies the precise roles played by the local angular velocity and the rotation of the strain axes in the alignment process and provides the framework in which to investigate the extent to which the straining field is 'persistent'. This general kinematical picture is specialized to study line and vortex stretching in fluid flows and analytically predicts the numerically observed alignment of the vorticity vector with the intermediate strain axis. The alignment equations are solved exactly for a number of special flow fields and investigated numerically for the ABC and STF flows. The kinematic formalism and numerical phenomenology suggests the use of new criteria to analyse the material element stretching properties of large-scale numerical simulations.

1. Introduction

The goal of this paper is to analyse, for quite general flow fields, the way in which material elements align with the local straining field and the subsequent degree of exponential stretching that ensues. Here the term 'material element' corresponds to the traditional concept of a collection of tagged fluid particles, each of which follows its own Lagrangian trajectory. In addition the material element, which here can be either one-dimensional (a line) or two-dimensional (a surface) is assumed to be passive; that is, it does not interact with the flow field. Apart from the obvious examples of threads of passive scalars such as temperature and dye, the stretching dynamics of material lines is a fundamental process relevant to understanding the stretching of vortex lines in ideal fluid flows and magnetic fields lines in ideal magnetohydrodynamic (MHD) flows. In addition, the deformation of infinitesimal material surfaces provides a model for propagating flame fronts. The alignment and stretching dynamics of lines is also useful in understanding the deformation of polymers, although they are not strictly passive, in turbulent flows – a vital issue in theories of drag reduction (Tabor & de Gennes 1986).

Our approach in this paper is primarily kinematic – that is, we will assume that the velocity field $\boldsymbol{u}(\boldsymbol{x}, t)$ is prescribed. Our aim is then to understand exactly which properties of $\boldsymbol{u}$ lead to the exponential stretching of material elements. Although we are primarily concerned with the fluid mechanical context and turbulent flows in particular, we are careful to separate results and insights for general flows from those of fluid dynamic significance. Thus, some of the concepts discussed here are also relevant to the analysis of three-dimensional chaotic dynamical systems in the large.

Although there have been many statistical theories of material element deformation in general and fluid flows (Batchelor 1952; Cocke 1969, 1971; Orszag 1970; Kraichnan 1970, 1974; Drummond & Münch 1990; Girimaji & Pope 1990), the kinematic details have apparently been somewhat neglected (Vieillefosse 1982, 1984; Majda 1991). In order to make precise comparisons with certain results of Girimaji & Pope and Vieillefosse we will, where appropriate, introduce the dynamical content of the Navier–Stokes equation into our kinematical formalism.

In studying the stretching process the traditional point of view has been to assume that the local straining field is 'persistent'. That is, the combined effects of vorticity and the rotation of the strain axes are small compared to the stretching effects of the principal shears themselves. This enables a material element to have time to align with the principal strain axis with the largest positive eigenvalue and hence experience the maximal, exponential stretching. The question of exactly how persistent the straining field of a given velocity field is, is an open one. The main aim of this paper is to provide the correct framework in which to study this fundamental problem and to give specific analytic and numerical examples illustrating this framework.

The assumption of persistent straining was made by Townsend (1951) in his study of the cooling of heat spots in decaying grid turbulence. Analytical estimates of the cooling rate, using this assumption, were found to be in good agreement with the experimental observations at mesh Reynolds numbers of several thousand. The first systematic treatment of the stretching of material elements in turbulent flows was given by Batchelor (1952) who made a number of important assumptions. The first was that a finite material element can be considered as a collection of infinitesimal elements since, in a turbulent flow, the stretching of elements separated by more than a few Kolomogorov lengths should be completely decorrelated. As long as one is averaging over many different material elements this appears to be a very reasonable assumption. This point of view will also be adopted here. It was also assumed that material points separate (continually) at an exponential rate (a rigorous demonstration of this, for finite times only, was provided much later by Cocke 1969) and a mean rate of exponential stretching was introduced. Although no assumptions about the persistence of the straining field were made in that paper the subsequent work of Batchelor & Townsend (1956) explicitly assumed persistence. This enabled the mean stretching rate to be identified with the mean of the largest eigenvalue of the rate of strain tensor (for which an estimate was given). Although there has, in fact, been little evidence to support the persistence-of-strain hypothesis (except for Townsend's experiment) it was sufficiently convenient to be adopted in many fluid dynamics problems (see, for example, Monn & Yaglom 1975).

Recently, however, various large-scale numerical simulations have cast doubt on this assumption. A study of the alignment of vorticity by Ashurst *et al.* (1987) showed that the vorticity tended to align with the strain axis with the intermediate eigenvalue rather than the direction with the largest eigenvalue – which should be the case (in ideal fluids) if the strain were persistent. An additional challenge has also been provided by Girimaji & Pope (1990) on the basis of their detailed studies of Lagrangian statistics in homogeneous isotropic turbulence at Taylor-scale Reynolds numbers of up to 90. They found the mean exponential stretching rate on a material line to be about one third of the Batchelor & Townsend result. This, coupled with other numerical tests, which we shall discuss later, indicated that the strain is not persistent.

This paper is organized as follows. In the next section we derive equations of

motion describing the alignment of a material element – lines, surfaces and vorticity – with the principal axes of strain. It is this rate-of-strain basis that provides the correct framework for analysing stretching and alignment phenomena as well as being the 'experimental' basis, i.e. the basis in which these phenomena are measured computationally. The equations of motion provide a precise quantification of the stretching rates of these material elements and the role which the local angular velocity (vorticity) and the rotation of the principal strain axes play in upsetting perfect alignment. In §3 we give the exact solutions to these equations for a variety of simple flow fields (namely, for various combinations of shears, and for extensional flow) and for the case of general two-dimensional flow we reduce the alignment equation to a particularly simple form. These analytical results give valuable insight into the details of the strain-basis rotation mechanism. In §4 we specialize our kinematic formalism to the case of material line and vortex stretching in fluid flows, relating the results of this work to those of Girimaji & Pope (1990) and Vieillefosse (1982, 1984). This study suggests new criteria for estimating the extent to which strain is or is not persistent and gives additional insight into why the tube-like regions of strong vorticity observed in turbulence simulations show strong alignment with the intermediate strain axis. In §5 we present numerical studies of the alignment dynamics for the ABC and STF flows. Despite their simplicity, the study of these flow fields (which are of considerable interest in dynamo theory) provides insight into the phenomenology of alignment dynamics for chaotic particle paths. In the last section we summarize our results and identify the remaining problems to be resolved.

2. Alignment kinematics

To obtain the desired alignment equation, we derive separate temporal evolution equations for material elements and for the principal directions of strain. Since this is a Lagrangian problem each fluid particle that makes up the material element is taken to follow its unique path determined by

$$\frac{\mathrm{d}}{\mathrm{d}t}\boldsymbol{x} = \boldsymbol{u}(\boldsymbol{x}(t), t), \quad \boldsymbol{x}(0) = \boldsymbol{x}_0, \quad \boldsymbol{u}, \boldsymbol{x}, \boldsymbol{x}_0 \in R^3. \tag{1}$$

Since it is infinitesimal, a material element, represented at time $t = 0$ by $\hat{\boldsymbol{l}}_0$, evolves according to the standard equation

$$\frac{\mathrm{d}}{\mathrm{d}t}\boldsymbol{l}(t) = (\boldsymbol{l}\cdot\nabla)\,\boldsymbol{u} = \boldsymbol{A}(t)\,\boldsymbol{l}(t), \quad \boldsymbol{l}(0) = \hat{\boldsymbol{l}}_0. \tag{2}$$

Here and throughout this paper $\boldsymbol{A}(t)$ denotes the velocity gradient tensor $\partial\boldsymbol{u}/\partial\boldsymbol{x}$, and $\boldsymbol{l}$ denotes a line element evolving according to (2). A surface element is represented as the vector product of two line elements $\boldsymbol{l}_1$ and $\boldsymbol{l}_2$ each of which evolves as a line element. The *instantaneous* exponential stretching rates for line and surface elements are given by (Batchelor 1952)

$$\zeta_{\mathrm{line}} = \frac{\mathrm{d}}{\mathrm{d}t}\log\|\boldsymbol{l}(t)\|, \tag{3}$$

$$\zeta_{\mathrm{surface}} = \frac{\mathrm{d}}{\mathrm{d}t}\log\|\boldsymbol{l}_1(t) \wedge \boldsymbol{l}_2(t)\| \tag{4}$$

(here $\boldsymbol{v}_1 \wedge \boldsymbol{v}_2$ is the vector product; $\|\boldsymbol{v}\|$ is the length of $\boldsymbol{v}$). The quantities $\bar{\zeta}_{\text{line}}$ and $\bar{\zeta}_{\text{surface}}$ correspond to *mean* stretching rates, where the overbar denotes a time average (equivalent to an ensemble average for ergodic flows).

Anticipating that the alignment of material element $\boldsymbol{l}(t)$ only concerns the direction of $\boldsymbol{l}(t)$, we introduce the *unit* vector $\hat{\boldsymbol{l}}(t)$ in the direction of $\boldsymbol{l}$ which evolves according to

$$\frac{\mathrm{d}}{\mathrm{d}t}\hat{\boldsymbol{l}} = \boldsymbol{A}\hat{\boldsymbol{l}} - \langle \hat{\boldsymbol{l}}, \boldsymbol{A}\hat{\boldsymbol{l}} \rangle \hat{\boldsymbol{l}}, \quad \hat{\boldsymbol{l}}(0) = \hat{\boldsymbol{l}}_0 \tag{5}$$

(here $\langle \boldsymbol{v}_1, \boldsymbol{v}_2 \rangle$ is the dot product). With this notation the instantaneous exponential separations can be expressed as

$$\zeta_{\text{line}} = \sum_{i,j} S_{ij} \hat{l}_i \hat{l}_j = \langle \hat{\boldsymbol{l}}, \boldsymbol{S}\hat{\boldsymbol{l}} \rangle, \tag{6}$$

$$\zeta_{\text{surface}} = \frac{\langle \hat{\boldsymbol{l}}_1, \boldsymbol{S}\hat{\boldsymbol{l}}_1 \rangle + \langle \hat{\boldsymbol{l}}_2, \boldsymbol{S}\hat{\boldsymbol{l}}_2 \rangle - 2\langle \hat{\boldsymbol{l}}_1, \hat{\boldsymbol{l}}_2 \rangle \langle \boldsymbol{S}\hat{\boldsymbol{l}}_1, \hat{\boldsymbol{l}}_2 \rangle}{1 - \langle \hat{\boldsymbol{l}}_1, \hat{\boldsymbol{l}}_2 \rangle^2}, \tag{7}$$

where $\boldsymbol{S}(t) = \frac{1}{2}(\boldsymbol{A} + \boldsymbol{A}^{\dagger})$ is the symmetric part of the velocity gradient tensor $\boldsymbol{A}(t)$ (i.e. the rate-of-strain tensor), and $\boldsymbol{A}^{\dagger}$ is the transpose of $\boldsymbol{A}$.

We now introduce the basis $\{\hat{\boldsymbol{\xi}}_1, \hat{\boldsymbol{\xi}}_2, \hat{\boldsymbol{\xi}}_3\}$ in which the strain tensor $\boldsymbol{S}(t)$ is diagonal. That is, we write $\boldsymbol{S}(t) = \boldsymbol{X}^{\dagger}\boldsymbol{D}\boldsymbol{X}$, where $\boldsymbol{X}$ is the matrix whose rows are the positively oriented ortho-normal eigenvectors (i.e. $\det \boldsymbol{X}(t) = +1$ for all times t). $\boldsymbol{D}$ is the matrix of eigenvalues $\operatorname{diag}\{s_1, s_2, s_3\}$ ordered so that $s_1 \geqslant s_2 \geqslant s_3$. In the context of fluid dynamical flows we shall also assume that the flow is incompressible (i.e. $s_1 + s_2 + s_3 = 0$) so that $s_1 \geqslant 0$ and $s_3 \leqslant 0$ for all times. The moving coordinate system in which $\boldsymbol{S}(t)$ is diagonal will be referred to as the *strain coordinates* or as the *strain basis*. In strain coordinates the stretching rate (6) becomes

$$\zeta_{\text{line}} = \sum_i s_i \lambda_i^2, \tag{8}$$

where $\hat{\boldsymbol{\lambda}} = \boldsymbol{X}\hat{\boldsymbol{l}}$ expressed in strain coordinates. Thus, λ_i is the cosine of the angle between $\hat{\boldsymbol{l}}$ and $\hat{\boldsymbol{\xi}}_i$. Equation (8) emphasizes the close connection between exponential stretching of material elements and their alignment with the principal axes of strain. Note that 'perfect alignment' for the line elements corresponds to $\hat{\boldsymbol{\lambda}} = (\pm 1, 0, 0)$ and $\zeta_{\text{line}} = s_1$ which is just the idealized persistence-of-strain hypothesis of Batchelor & Townsend. Perfect alignment for material surfaces corresponds to $\hat{\boldsymbol{\lambda}}_1 = \hat{\boldsymbol{\xi}}_1$ and $\hat{\boldsymbol{\lambda}}_2 = \hat{\boldsymbol{\xi}}_2$ and, hence, $\zeta_{\text{surface}} = s_1 + s_2$ (Batchelor 1952).

To obtain the evolution equation for the components of $\hat{\boldsymbol{\lambda}}$ we require evolution equations for both the material element and for the basis of eigenvectors. Starting from

$$\frac{\mathrm{d}}{\mathrm{d}t}\lambda_i = \left\langle \frac{\mathrm{d}}{\mathrm{d}t}\hat{\boldsymbol{l}}, \hat{\boldsymbol{\xi}}_i \right\rangle + \left\langle \hat{\boldsymbol{l}}, \frac{\mathrm{d}}{\mathrm{d}t}\hat{\boldsymbol{\xi}}_i \right\rangle, \tag{9}$$

we can use (5) on the first term, but must now derive an equation governing the evolution of the eigenvectors. Requiring orthonormality of the principal axes, $\langle \hat{\boldsymbol{\xi}}_i, \hat{\boldsymbol{\xi}}_j \rangle = \delta_{ij}$, guarantees that $\langle (\mathrm{d}/\mathrm{d}t)\hat{\boldsymbol{\xi}}_i, \hat{\boldsymbol{\xi}}_j \rangle = 0$ for all times and, hence, that

$$\frac{\mathrm{d}}{\mathrm{d}t}\hat{\boldsymbol{\xi}}_i = \boldsymbol{\Omega}'(t) \wedge \hat{\boldsymbol{\xi}}_i, \tag{10}$$

for some vector $\boldsymbol{\Omega}'(t)$. The vector $\boldsymbol{\Omega}'(t)$ is the *instantaneous* axis of rotation for the principal axes of strain and we shall refer to it as the *strain rotation vector* (a more compact term might be the 'orienticity'). To calculate the components of $\boldsymbol{\Omega}'$, we differentiate the characteristic equation $\boldsymbol{S}\hat{\boldsymbol{\xi}}_j = s_j\hat{\boldsymbol{\xi}}_j$ with respect to time, take the inner product of both sides with $\hat{\boldsymbol{\xi}}_i$, use (10), and obtain the result

$$\Omega'_k = \epsilon_{ijk}\frac{\langle\hat{\boldsymbol{\xi}}_i, \dot{\boldsymbol{S}}\hat{\boldsymbol{\xi}}_j\rangle}{s_i - s_j} \quad \text{(no summation)} \tag{11}$$

(here ϵ_{ijk} is the usual three dimensional totally antisymmetric tensor, and the over-dot denotes total time differentiation). It should be noted that (11) gives $\boldsymbol{\Omega}'$ in strain coordinates and that $\boldsymbol{\Omega}'$ depends on the dynamic evolution of the velocity field via $\dot{\boldsymbol{S}}$. In the fluid dynamical setting this evolution equation for $\dot{\boldsymbol{S}}$ is just the symmetric gradient of the Navier–Stokes equation. We will always assume that $\boldsymbol{\Omega}'$ is finite as the principal shears become degenerate. This is shown explicitly in two dimensions (see the Appendix). The assumed finiteness of $\boldsymbol{\Omega}'$, the condition $\det\boldsymbol{X}(t) = +1$, and the ordering $s_1 \geqslant s_2 \geqslant s_3$ ensure that the eigenvector matrix $\boldsymbol{X}(t)$ is well-defined and unique for all times (i.e. that $\boldsymbol{X}(0)$ determines $\boldsymbol{X}(t)$ for all times).

Now (9) becomes

$$\frac{\mathrm{d}}{\mathrm{d}t}\hat{\boldsymbol{\lambda}} = \begin{pmatrix} s_1 & 0 & 0 \\ 0 & s_2 & 0 \\ 0 & 0 & s_3 \end{pmatrix}\hat{\boldsymbol{\lambda}} - \zeta_{\text{line}}\hat{\boldsymbol{\lambda}} + (\boldsymbol{\Omega} - \boldsymbol{\Omega}') \wedge \hat{\boldsymbol{\lambda}}, \quad \hat{\boldsymbol{\lambda}}(0) = \boldsymbol{X}\hat{\boldsymbol{l}}_0, \tag{12}$$

where $\boldsymbol{\Omega}$ is the angular velocity of the local fluid element, i.e. $\boldsymbol{\Omega} = \frac{1}{2}\boldsymbol{\nabla} \wedge \boldsymbol{u}$ (to be distinguished from the actual vorticity $\boldsymbol{\omega} = \boldsymbol{\nabla} \wedge \boldsymbol{u}$) and ζ_{line} is the instantaneous stretching rate given by (8). Thus, the second term in (12) is nonlinear. Noting that the angular velocity and strain rotation appear together in (12) we define the vector $\boldsymbol{\mathcal{R}} = \boldsymbol{\Omega} - \boldsymbol{\Omega}'$ which we call the *effective rotation*. In strain coordinates the material element sees the rotating effect of angular velocity $\boldsymbol{\Omega}$ and eigenvector rotation $\boldsymbol{\Omega}'$ as if the angular velocity were replaced by $\boldsymbol{\mathcal{R}}$ and the eigenvectors were stationary ($\boldsymbol{\Omega}' = \boldsymbol{0}$). The terms in the alignment equation are interpreted as follows. The first two terms in (12) exponentially attract the material element $\hat{\boldsymbol{\lambda}}$ into alignment with the principal direction, $\hat{\boldsymbol{\xi}}_1$, corresponding to the largest strain; the last term instantaneously rotates it about the axis $\boldsymbol{\mathcal{R}}$ with angular velocity $\|\boldsymbol{\mathcal{R}}\|$. The rotating effect of this term is clear; the aligning effect of the first two term is seen as follows.

If we isolate the alignment terms of (12) by assuming that the first two terms are dominant (i.e. $\boldsymbol{\mathcal{R}} \approx \boldsymbol{0}$) and set $\eta_i = s_i - \zeta_{\text{line}}$, equation (12) becomes

$$\frac{\mathrm{d}}{\mathrm{d}t}\lambda_i = \eta_i\lambda_i. \tag{13}$$

In this form the components of the material element are seen to instantaneously either grow or shrink exponentially. Incompressibility, the ordering $s_1 \geqslant s_2 \geqslant s_3$, and the condition $\zeta_{\text{line}} \leqslant s_1$ immediately gives the inequalities

$$\eta_1 \geqslant 0, \quad \eta_1 \geqslant \eta_2 \geqslant \eta_3, \quad \eta_3 \leqslant 0. \tag{14}$$

Thus, $\lambda_1(t)$ monotonically grows to ± 1 and $\lambda_3(t)$ monotonically shrinks to 0. The only complexity lies in the behaviour of $\lambda_2(t)$. All we can say about λ_2 is that its growth/decay rate η_2 has the same instantaneous sign as s_2. This is seen as follows.

After transients of the material element's initial condition have died out, (14) will ensure that

$$\lambda_1^2(t) \geqslant \lambda_2^2(t) \geqslant \lambda_3^2(t) \tag{15}$$

for all subsequent times. Then, assuming $s_2(t)$ is positive we have

$$\begin{aligned} \eta_2 &= s_2 - s_2\lambda_2^2 - s_1\lambda_1^2 - s_3\lambda_3^2 \\ &\geqslant -s_1\lambda_1^2 - s_3\lambda_3^2 \geqslant -(s_1+s_3)\lambda_3^2 = s_2\lambda_3^2 \geqslant 0. \end{aligned} \tag{16}$$

Similarly, if $s_2(t)$ is negative we conclude that $\eta_2 \leqslant 0$. In the absence of rotation, $\mathscr{R} = \mathbf{0}$, the instantaneous sign of $s_2(t)$ determines the growth/decay of λ_2 and, hence, how quickly $\hat{\boldsymbol{\lambda}}$ reaches the state of 'perfect' alignment. According to the time-averaged sign of $s_2(t)$ there will be two alignment paradigms: 'efficient' and 'inefficient' alignment. Inefficient alignment is characterized by $\bar{s}_2 > 0$ in which, on average, the material line is attracted to both the $\hat{\boldsymbol{\xi}}_1$ and $\hat{\boldsymbol{\xi}}_2$ directions. On the other hand, efficient alignment is characterized by $\bar{s}_2 < 0$. Here only the $\hat{\boldsymbol{\xi}}_1$ direction attracts the material line. Analytical arguments (Betchov 1956) and numerical results (Ashurst *et al.* 1987) independently suggest that the average value $\bar{s}_2$ is positive for idealized turbulence. This suggests that the state of inefficient alignment should be typical and that the rate of stretching should be significantly reduced (ignoring rotational effects).

The fixed points of the alignment equation with $\mathscr{R} = \mathbf{0}$ are $\hat{\boldsymbol{\lambda}}^{(1)} = (\pm 1, 0, 0)$, $\hat{\boldsymbol{\lambda}}^{(2)} = (0, \pm 1, 0)$, and $\hat{\boldsymbol{\lambda}}^{(3)} = (0, 0, \pm 1)$. Only $\hat{\boldsymbol{\lambda}}^{(1)}$, i.e. the perfect alignment state, is a stable fixed point of equation (12) with $\mathscr{R} = \mathbf{0}$; both $\hat{\boldsymbol{\lambda}}^{(2)}$ and $\hat{\boldsymbol{\lambda}}^{(3)}$ are unstable. Study of the fixed points and stability properties of the alignment equation for $\mathscr{R} \neq \mathbf{0}$ is an important problem worthy of further investigation.

For non-zero $\mathscr{R}$ the typical situation may well be that strong angular velocity or strain rotation, or both, conspire to unpredictably upset the aligning efforts of the first two terms of (12). The numerical integrations of the alignment equation discussed in §5 certainly display this feature. Inspecting (12) we would expect that in the limit in which the rotation term is much stronger than the aligning terms (i.e. $\mathscr{R}_i \gg s_i$) the material element will rapidly rotate about the instantaneous rotation vector $\mathscr{R}$. Hence there will be a nearly vanishing mean exponential stretching rate ζ_{line} as long as the vector $\mathscr{R}$ itself has no special alignment properties. If $\mathscr{R}$ does have special alignment properties, as may be the case for fluid flows, the situation is more complex. These complexities are not present in material line stretching in two dimensions where the vorticity and strain rotation are constrained to point in one direction (the direction out of the plane of motion) and where we expect that the $\mathscr{R} \gg \boldsymbol{s}$ limit exactly differentiates cases of minimal and maximal persistence of strain. We will see this explicitly in §3.

We conclude this section by discussing general features of the alignment equation (12) for vorticity in ideal fluid flows. The angular velocity (vorticity) evolves for ideal flows as the curl of the Euler equations

$$\frac{\mathrm{d}}{\mathrm{d}t}\boldsymbol{\Omega} = \partial_t \boldsymbol{\Omega} + (\boldsymbol{u}\cdot\nabla)\boldsymbol{\Omega} = (\boldsymbol{\Omega}\cdot\nabla)\boldsymbol{u} = A(t)\,\boldsymbol{\Omega}. \tag{17}$$

This is identical in form to the evolution equation for material lines, (2). As before we introduce the unit-length vorticity in the strain basis $\hat{\boldsymbol{\Omega}}$ and the vorticity exponential stretching rate $\zeta_{\text{vorticity}}$ so that

$$\zeta_{\text{vorticity}} = \langle \hat{\boldsymbol{\Omega}}, \boldsymbol{S}\hat{\boldsymbol{\Omega}} \rangle = \sum_i s_i \hat{\Omega}_i^2. \tag{18}$$

The alignment equation for vorticity becomes

$$\frac{\mathrm{d}}{\mathrm{d}t}\hat{\boldsymbol{\Omega}} = \begin{pmatrix} s_1 & 0 & 0 \\ 0 & s_2 & 0 \\ 0 & 0 & s_3 \end{pmatrix}\hat{\boldsymbol{\Omega}} - \zeta_{\text{vorticity}}\,\hat{\boldsymbol{\Omega}} - \boldsymbol{\Omega}' \wedge \hat{\boldsymbol{\Omega}}. \tag{19}$$

The angular velocity $\boldsymbol{\Omega}$ is absent here because $\boldsymbol{\Omega} \wedge \hat{\boldsymbol{\Omega}}$ vanishes identically. The absence of this term distinguishes material line and vorticity stretching (compare (12) with (19)). Since, in general, we interpret effects of rotation as denying the material element a chance to align with the principal stretching directions we would expect the absence of this term to cause material lines to stretch less than vorticity itself.

We now compare the relative extents of possible line element stretching and vorticity stretching. In the case of the latter let us suppose that the vorticity (and hence $\boldsymbol{\Omega}$) aligns to some extent with both $\hat{\boldsymbol{\xi}}_1$ and $\hat{\boldsymbol{\xi}}_2$, i.e. we write

$$\boldsymbol{\Omega} \approx \Omega_1 \hat{\boldsymbol{\xi}}_1 + \Omega_2 \hat{\boldsymbol{\xi}}_2 \tag{20}$$

(the results of Ashurst *et al.* suggest, in fact, that on average $\Omega_2 > \Omega_1$). In a similar vein, for line element stretching, we can write

$$\hat{\boldsymbol{\lambda}} \approx \lambda_1 \hat{\boldsymbol{\xi}}_1 + \lambda_2 \hat{\boldsymbol{\xi}}_2 \tag{21}$$

(for persistent strain λ_1 is significantly larger than λ_2). Comparing the line element (12) and vorticity (19) alignment equations, the only difference between these two processes lies in the term

$$\boldsymbol{\Omega} \wedge \hat{\boldsymbol{\lambda}} \approx (\Omega_1 \lambda_2 - \Omega_2 \lambda_1)\hat{\boldsymbol{\xi}}_3. \tag{22}$$

From this we immediately see two interesting limits. One corresponds to the (experimentally) inconsistent case of both $\boldsymbol{\Omega}$ and $\hat{\boldsymbol{\lambda}}$ aligning with $\hat{\boldsymbol{\xi}}_1$. This would lead to a small value of $\boldsymbol{\Omega} \wedge \hat{\boldsymbol{\lambda}}$ with the consequence that the $\hat{\boldsymbol{\lambda}}$ and $\hat{\boldsymbol{\Omega}}$ alignment equations are approximately the same and hence $\bar{\zeta}_{\text{line}} \approx \bar{\zeta}_{\text{vorticity}}$. The other, (experimentally) more consistent limit, corresponds to $\boldsymbol{\Omega}$ aligning with $\hat{\boldsymbol{\xi}}_2$ and $\hat{\boldsymbol{\lambda}}$ aligning with $\hat{\boldsymbol{\xi}}_1$ (even if the strain is not fully persistent) and hence a more significant contribution from $\boldsymbol{\Omega} \wedge \hat{\boldsymbol{\lambda}}$. This contribution takes the form of fluctuations in λ_3 (see (12)) which will result, since $s_3\lambda_3^2$ is negative definite, in $\bar{\zeta}_{\text{line}} < \bar{\zeta}_{\text{vorticity}}$. This prediction should be measurable using direct numerical simulation techniques. (It should also be possible to give analogous kinematic arguments to compare $\bar{\zeta}_{\text{line}}$ with $\bar{\zeta}_{\text{surface}}$.)

3. Exact solutions for simple flow fields

In this section we present exact solutions to the alignment equation (12) for velocity gradient tensors of several different forms. The first example will be extensional flow. The second will consist of two increasingly general shear flows. Our third example will be general two-dimensional flows. The utility of these exact solutions is primarily illustrative but does provide valuable insight into behaviour in the strain basis. For general three-dimensional velocity gradient tensors, the difficulties of analytically solving the alignment equation explicitly are substantial and can only be overcome by choosing forms of the velocity gradient tensor which are easily diagonalized.

Incompressible extensional flow,

$$\boldsymbol{A}(t) = \begin{pmatrix} s_1 & 0 & 0 \\ 0 & s_2 & 0 \\ 0 & 0 & -(s_1+s_2) \end{pmatrix}, \tag{23}$$

gives the same qualitative features of the alignment term of (12) in the limit of a vanishing rotation term. That is, extensional flow asymptotically reaches perfect alignment. For extensional flows there is no angular velocity or eigenvector rotation. The alignment equation can be written in the form

$$\left.\begin{aligned} \frac{\mathrm{d}}{\mathrm{d}t}\log(\lambda_2/\lambda_1) &= -(s_1-s_2) \leqslant 0, \\ \frac{\mathrm{d}}{\mathrm{d}t}\log(\lambda_3/\lambda_1) &= -(2s_1+s_2) \leqslant 0, \end{aligned}\right\} \tag{24}$$

which gives $\lambda_2(t)$ and $\lambda_3(t)$ in terms of $\lambda_1(t)$:

$$\left.\begin{aligned} \lambda_2(t) &= \frac{\lambda_2(0)}{\lambda_1(0)}\lambda_1(t)\exp\left(\int_0^t -(s_1(t')-s_2(t'))\,\mathrm{d}t'\right), \\ \lambda_3(t) &= \frac{\lambda_3(0)}{\lambda_1(0)}\lambda_1(t)\exp\left(\int_0^t -(2s_1(t')+s_2(t'))\,\mathrm{d}t'\right). \end{aligned}\right\} \tag{25}$$

The negativity of the right-hand sides of (24) then ensures that λ_1 and λ_3 exponentially go to zero and hence that λ_1 approaches ± 1 as t becomes large. The state of perfect alignment is reached exponentially, and once reached the stretching rates satisfy

$$\zeta_{\text{line}}(\tau), \zeta_{\text{vorticity}}(\tau) \sim s_1(\tau), \quad \zeta_{\text{surface}}(\tau) \sim s_1(\tau)+s_2(\tau) \tag{26}$$

for large τ.

Next, we solve the case of a single shear flow,

$$\boldsymbol{A}(t) = \begin{pmatrix} 0 & a(t) & 0 \\ 0 & 0 & 0 \\ 0 & 0 & 0 \end{pmatrix}, \tag{27}$$

where $a(t)$ is the shear $\partial u_x/\partial y$ evaluated along the Lagrangian path. This flow will have the effect of pushing the material vector away from the y-direction, so that it will eventually align with the direction of fluid flow (in this case the x-axis). At any instant in time, $\boldsymbol{l}$ will align with the either the x-axis or the $-x$-axis depending on the instantaneous sign of $a(t)$. This qualitative behaviour is most clearly seen out of the strain basis. The Cartesian evolution equation for the material vector, (2), can be readily solved to give

$$l_x(t) = \left(\int_0^t a(t')\,\mathrm{d}t'\right) l_y(0), \quad l_y(t) = l_y(0), \quad l_z(t) = l_z(0). \tag{28}$$

It is clear here how the instantaneous sign of $a(t)$ determines the small-time increase or decrease of l_x. As a prelude to things to come, we now repeat this result in the strain basis. The principal shears are $s_1 = \frac{1}{2}|a|$, $s_2 = 0$, $s_3 = -\frac{1}{2}|a|$; the corresponding orthonormal, positively oriented eigenvectors are

$$\hat{\boldsymbol{\xi}}_1 = \frac{\sigma}{\sqrt{2}}(1,1,0), \quad \hat{\boldsymbol{\xi}}_2 = (0,0,1), \quad \hat{\boldsymbol{\xi}}_3 = \frac{\sigma}{\sqrt{2}}(1,-1,0), \tag{29}$$

where $\sigma(t)$ is the instantaneous sign of $a(t)$. At any instant in time the eigenvectors are stationary. Thus, the shear rotation vector is zero and the rotation $\mathscr{R}$ is just the

angular velocity written in the strain basis, i.e. $\mathscr{R}(t) = \boldsymbol{X\Omega} = (0, -\frac{1}{2}a(t), 0)$. By changing variables to

$$\alpha = \frac{1}{\sqrt{2}}(\lambda_1+\lambda_3), \quad \beta = \frac{1}{\sqrt{2}}(\lambda_1-\lambda_3), \quad \gamma = \lambda_2, \tag{30}$$

and introducing the monotonically increasing time variable

$$\tau(t) = \int_0^t |a(t')|\,\mathrm{d}t', \tag{31}$$

we transform the alignment equation (12) into

$$\frac{\mathrm{d}\alpha}{\mathrm{d}\tau} = \beta\left(\frac{1+\sigma}{2}-\alpha^2\right), \quad \frac{\mathrm{d}\beta}{\mathrm{d}\tau} = \alpha\left(\frac{1-\sigma}{2}-\beta^2\right), \quad \frac{\mathrm{d}\gamma}{\mathrm{d}\tau} = -\alpha\beta\gamma. \tag{32}$$

Since these equations are invariant under the transformation $(\alpha, \beta, \sigma) \mapsto (\beta, \alpha, -\sigma)$, we may assume that $\sigma = +1$. Hence we can solve the resulting equations and apply this invariance to obtain the solution for $\sigma = -1$. The relation $1 = \|\hat{\boldsymbol{\lambda}}\| = \alpha^2+\beta^2+\gamma^2$ suggests the use of spherical coordinates

$$\alpha = \cos\theta, \quad \beta = \sin\theta\cos\phi, \quad \gamma = \sin\theta\sin\phi \tag{33}$$

which reduce the alignment equation, with $\sigma = +1$, to the exactly solvable form

$$\frac{\mathrm{d}\theta}{\mathrm{d}\tau} = -\sin^2\theta\cos\phi, \quad \frac{\mathrm{d}\phi}{\mathrm{d}\tau} = 0. \tag{34}$$

The solution is then

$$\frac{\alpha}{\beta} = \frac{\alpha_0}{\beta_0}\tau, \quad \frac{\gamma}{\beta} = \frac{\gamma_0}{\beta_0}, \tag{35}$$

given initial conditions α_0, β_0, and γ_0. As long as $a(t)$ is positive ($\sigma = +1$) the material line approaches the state $\beta, \gamma \sim 0$ and $\alpha \sim \pm 1$ as $t \to \infty$, corresponding to alignment with the x-axis. (This is the only possibility since α, β, and γ must all be bounded.) While $a(t)$ is negative the $\sigma = -1$ solution leads to $\alpha, \gamma \sim 0$ and $\beta \sim \pm 1$ as $t \to \infty$. Thus, $\sigma = -1$ leads to alignment with the $-x$-axis. If we take the shear a to be constant, σ is fixed and we get either $\alpha, \gamma \sim 1/t$ or $\beta, \gamma \sim 1/t$ (depending on whether $\sigma = +1$ or $\sigma = -1$). Since this asymptotic approach of the x-axis is algebraic we expect the mean exponential separation to be zero. This result will be made explicit in what follows.

The case of the two-shear flow,

$$\boldsymbol{A}(t) = \begin{pmatrix} 0 & a(t) & b(t) \\ 0 & 0 & 0 \\ 0 & 0 & 0 \end{pmatrix}, \tag{36}$$

is qualitatively very similar to the single-shear flow and is also exactly soluble. Here $a(t)$ and $b(t)$ are, respectively, $\partial u_x/\partial y$ and $\partial u_x/\partial z$ evaluated along the Lagrangian path. Intuitively, the flow pushes the material element away from both the y- and z-directions, so that as long as a and b are monotone increasing or decreasing we expect alignment with the x- or $-x$-axis, respectively. Again, this is most easily seen by solving the Cartesian evolution equation for $\boldsymbol{l}$ to obtain

$$l_x(t) = \left(\int_0^t a(t')\,\mathrm{d}t'\right) l_y(0) + \left(\int_0^t b(t')\,\mathrm{d}t'\right) l_z(0), \quad l_y(t) = l_y(0), \quad l_z(t) = l_z(0). \tag{37}$$

Unlike the single-shear flow, however, here the principal axes are moving, so that although we know that alignment can only happen asymptotically with the $\pm x$-axis, it is not clear *a priori* what happens in the strain basis. We proceed now in the strain basis. The principal shears are $s_1 = \frac{1}{2}c$, $s_2 = 0$, $s_3 = -\frac{1}{2}c$, where $c^2 = a^2 + b^2$. The principal directions are

$$\hat{\xi}_1 = \frac{1}{\sqrt{2}}\left(1, \frac{a}{c}, \frac{b}{c}\right), \quad \hat{\xi}_2 = \left(0, -\frac{b}{c}, \frac{a}{c}\right), \quad \hat{\xi}_3 = \frac{1}{\sqrt{2}}\left(1, -\frac{a}{c}, -\frac{b}{c}\right).$$

In strain coordinates the angular velocity is $\boldsymbol{\Omega} = (0, -\frac{1}{2}c(t), 0)$. The strain rotation is

$$\boldsymbol{\Omega}' = \frac{1}{\sqrt{2}} c\kappa(1, 0, 1),$$

where κ is the curvature of the curve with velocity vector $(a(t), b(t))$ in the (a, b)-plane

$$\kappa(t) = \frac{a\dot{b} - b\dot{a}}{(a^2 + b^2)^{\frac{3}{2}}}.$$

Once again using the coordinates defined by (30) as well as the analogous monotonically increasing time variable

$$\tau(t) = \int_0^t |c(t')| \, \mathrm{d}t', \tag{38}$$

the alignment equation becomes

$$\frac{\mathrm{d}\alpha}{\mathrm{d}\tau} = \beta(1 - \alpha^2), \quad \frac{\mathrm{d}\beta}{\mathrm{d}\tau} = -\alpha\beta^2 + \kappa\gamma, \quad \frac{\mathrm{d}\gamma}{\mathrm{d}\tau} = -\alpha\beta\gamma - \kappa\beta. \tag{39}$$

One can see that the only steady-state solution of (39) is $\alpha = \pm 1$ and $\beta = \gamma = 0$ (i.e. alignment with the $\pm x$-axis). So, if any alignment is to persist it must be made with the $\pm x$-axis. Again using the spherical coordinates (33) we obtain the two equations

$$\frac{\mathrm{d}\theta}{\mathrm{d}\tau} = -\sin^2\theta \cos\phi, \quad \frac{\mathrm{d}\phi}{\mathrm{d}\tau} = -\kappa(\tau). \tag{40}$$

Solving these equations with initial conditions α_0, β_0, γ_0 and $\tan\phi_0 = \gamma_0/\beta_0$, one obtains

$$\left.\begin{aligned} \frac{\alpha(t)}{(\beta(t)^2 + \gamma(t)^2)^{\frac{1}{2}}} - \frac{\alpha_0}{(\beta_0^2 + \gamma_0^2)^{\frac{1}{2}}} &= \int_0^\tau \cos\phi(\tau') \, \mathrm{d}\tau', \\ \frac{\gamma(t)}{\beta(t)} - \frac{\gamma_0}{\beta_0} &= \frac{r(t) - r_0}{r(t)\, r_0 + 1}. \end{aligned}\right\} \tag{41}$$

We have introduced the ratio $r(t) = a(t)/b(t)$ and note that the solution depends on a and b only through their ratio. To characterize this solution we study those particular forms of the functions a and b which lead to the steady-state alignment with the x-axis. The only way in which steady state can be reached is for the integral

$$\int_0^\tau \cos\phi(\tau') \, \mathrm{d}\tau' = \int_0^\tau \cos(\phi - \phi_0)\left(\cos\phi_0 - \frac{r - r_0}{r r_0 + 1} \sin\phi_0\right) \mathrm{d}\tau' \tag{42}$$

to be monotone increasing or decreasing. Since $\cos\phi$ is always between -1 and 1 this

will happen if it takes on one sign more frequently than the other sign. Thus, if $\cos\phi$ is periodic in τ no alignment with the $\pm x$-axis will be attained. Another way of expressing this is as follows. If the zeros of the integrand, which occur whenever

$$r(t) = -\frac{1}{r_0} = -\frac{b_0}{a_0} \quad \text{and} \quad r(t) = \frac{1+r_0\tan\phi_0}{\tan\phi_0 - r_0} = \frac{\beta_0 b_0 + a_0\gamma_0}{\gamma_0 b_0 - a_0 b_0}, \tag{43}$$

are crossed with equal frequency in time then alignment (with the x-axis) will be suppressed. Note that all features here are highly dependent on both the initial conditions of $\hat{\boldsymbol{\lambda}}$ (via α_0, β_0, and γ_0) as well as the initial conditions of the shears a_0 and b_0. The shear flows studied here have a strong memory of their initial conditions. This strong memory should certainly be lost for chaotic particle paths.

If a and b are both constant, (41) reduces to

$$\gamma(t)/\beta(t) = \gamma_0/\beta_0, \quad \alpha(t)\,\gamma_0/\gamma(t) = \alpha_0 + t[c(\beta_0^2+\gamma_0^2)^{\frac{1}{2}}\cos\phi_0]. \tag{44}$$

This can only be satisfied for large t if $\alpha \sim \pm 1$ and $\beta, \gamma \sim 1/t$. Thus, constant a and b leads to asymptotic algebraic alignment with the $\pm x$-axis.

This algebraic alignment would lead us to believe that the mean exponential stretching should be zero for the two-shear flow with constant shears a and b. In fact, the exponential separation is zero for general time-dependent $a(t)$ and $b(t)$, as we shall now show. The exponential separation can be written $\zeta_{\text{line}}(t) = 2c\alpha\beta$. The time-averaged line separation can be seen to be zero as follows:

$$\bar{\zeta}_{\text{line}} = 2\lim_{T\to\infty}\frac{1}{T}\int_0^T \alpha(\tau)\,\beta(\tau)\,\mathrm{d}\tau \tag{45}$$

$$= -2\lim_{T\to\infty}\frac{1}{T}\int_{\theta(0)}^{\theta(T)}\frac{\cos\theta}{\sin\theta}\mathrm{d}\theta = -2\lim_{T\to\infty}\frac{1}{T}\log\sin\theta(T) = 0. \tag{46}$$

(Here we have used the monotonicity of τ as well as (40) in the form $\sin^2\theta\,\mathrm{d}\theta = -\cos\phi\,\mathrm{d}\phi$.) If we make the plausible assumption that turbulent flows exhibit some degree of positive exponential separation (Cocke 1969) then, by comparison, the two-shear flows studied here can be thought of as examples of flows with the 'worst' alignment properties.

The alignment equation for general two-dimensional flows can be reduced to a very simple equation. Here, the gradient tensor is written in the form

$$\boldsymbol{A}(t) = \begin{pmatrix} c+a & b+\Omega \\ b-\Omega & c-a \end{pmatrix}, \tag{47}$$

where $a(t)$, $b(t)$, $c(t)$ and $\Omega(t)$ are given functions of time t. We can also consider compressible flows ($c = \frac{1}{2}\nabla\cdot\boldsymbol{u} \neq 0$) here because we will find that c does not enter the alignment equation. One obtains the angular velocity $\boldsymbol{\Omega} = \Omega\hat{\boldsymbol{z}}$ ($\hat{\boldsymbol{z}}$ is the unit vector normal to the plane) and shears $s_\pm = c \pm \gamma$ where $\gamma^2 = a^2 + b^2$. The shear basis is $\{\hat{\boldsymbol{\xi}}_+, \hat{\boldsymbol{\xi}}_-\}$ where

$$\hat{\boldsymbol{\xi}}_\pm = \frac{1}{[2\gamma(\gamma \mp a)]^{\frac{1}{2}}}\begin{pmatrix} b \\ -a \pm \gamma \end{pmatrix}. \tag{48}$$

The eigenvector rotation is

$$\boldsymbol{\Omega}' = \frac{1}{2}\frac{\dot{a}b - a\dot{b}}{a^2+b^2}\hat{\boldsymbol{k}}. \tag{49}$$

If λ_+ and λ_- are the cosines of the angles between $\hat{\lambda}$ and the principal directions $\hat{\xi}_\pm$, we choose the coordinates $\alpha_\pm = (\lambda_+ \pm \lambda_-)/\sqrt{2}$, and define the monotonic time

$$\tau(t) = 2\int_0^t \gamma(t')\,\mathrm{d}t', \tag{50}$$

the alignment equation becomes

$$\frac{\mathrm{d}\alpha_+}{\mathrm{d}\tau} = \tfrac{1}{2}(1+r)\,\alpha_- - \alpha_+^2\,\alpha_-, \quad \frac{\mathrm{d}\alpha_-}{\mathrm{d}\tau} = \tfrac{1}{2}(1-r)\,\alpha_+ - \alpha_-^2\,\alpha_+. \tag{51}$$

This equation only depends on the flow fields through the parameter $r(\tau) = (\Omega' - \Omega)/\gamma$ (i.e. the ratio between the effective rotation and the difference between the shears). Furthermore, r is independent of the compressibility c. Since $\alpha_+^2 + \alpha_-^2 = 1$ for all times we use the polar coordinates

$$\alpha_+ = \cos(\tfrac{1}{2}\theta), \quad \alpha_- = \sin(\tfrac{1}{2}\theta) \tag{52}$$

and transform the alignment equation into

$$\frac{\mathrm{d}\theta}{\mathrm{d}\tau} - \cos\theta = r(\tau). \tag{53}$$

Although this equation appears not to be exactly soluble for general $r(\tau)$ it is probably amenable to numerical simulations. Further work is needed to explore this and other possibilities. The mean line stretching rate can be written in the form

$$\bar{\zeta}_{\mathrm{line}} = \bar{c} - \frac{1}{2}\lim_{T\to\infty}\frac{1}{T}\int_0^T \sin\theta(\tau)\,\mathrm{d}\tau. \tag{54}$$

It is interesting to note that for compressible two-dimensional fluid flow fields, the compressibility $\bar{c} = (\mathrm{d}/\mathrm{d}t)\log\rho$ and hence time averages to zero. For incompressible flows we can see exactly how the limits $|r| \ll 1$ and $|r| \gg 1$ respectively lead to maximal and minimal persistence of strain. Recall that the large and small rotation-versus-shear limits were discussed above in the context of general flow fields. Here we can see exactly how these limits are manifested. When $|r| \ll 1$, (53) is exactly soluble leading to exponentially achieved perfect alignment. On the other hand when $|r| \gg 1$, $\theta(\tau)$ can be seen to be a rapidly varying function of τ so that $\sin\theta$ will oscillate quickly and average to zero. Thus, the persistence of strain in two-dimensional fluid flows can be characterized with a single number. In three dimensions the situation is considerably more complex.

4. Line and vortex stretching in fluid flows

We now consider material line and vorticity stretching in incompressible fluid flows by introducing the dynamics of the Navier–Stokes equations into our kinematic formalism. Our aim here is to illustrate the utility of the strain-basis kinematic formalism – especially as it relates to the work of Vieillefosse (1982, 1984) and Girimaji & Pope (1990). In specializing the general alignment equation (12) to the particular case of fluid flows it is important to note that this general equation depends on three classes of external time-dependent quantities: the principal shears (s_1, s_2, and s_3), the angular velocity (vorticity) $\boldsymbol{\Omega}$ and the eigenvector rotation $\boldsymbol{\Omega}'$ as defined by (11). These external quantities are either derived explicitly, as is the case

for the exact solution and numerical model velocity fields of §§3 and 5, or are themselves governed by evolution equations, as is the case here. For a viscous fluid the local angular velocity evolves according to the curl of the Navier–Stokes equation

$$\frac{\mathrm{d}}{\mathrm{d}t}\boldsymbol{\Omega}(\boldsymbol{x},t) = \boldsymbol{S}\boldsymbol{\Omega} + \nu\nabla^2\boldsymbol{\Omega}, \tag{55}$$

and itself evolves as a material line in the limit of vanishing kinematic viscosity ν (cf. (2)). The symmetric gradient of the Navier–Stokes equation,

$$\frac{\mathrm{d}}{\mathrm{d}t}\boldsymbol{S}(\boldsymbol{x},t) = -(\boldsymbol{S}^2 + \tilde{\boldsymbol{\Omega}}^2) - \boldsymbol{P} + \nu\nabla^2\boldsymbol{S}, \tag{56}$$

determines the evolution of the principal shears. Here $\tilde{\boldsymbol{\Omega}}$ denotes the vorticity tensor $\frac{1}{2}(\boldsymbol{A}(t) - \boldsymbol{A}^{\mathrm{T}}(t))$, and $\boldsymbol{P}(t)$ denotes the pressure second-derivative tensor, both evaluated along a fluid particle path. This leads to an expression for the local eigenvector rotation in the strain basis:

$$\Omega'_k(t) = \epsilon_{ijk}\left(\frac{-\Omega_i\Omega_j - P_{ij} + \nu(\nabla^2 S)_{ij}}{s_i - s_j}\right). \tag{57}$$

From (57) it is evident that the total strain rotation vector can be split into three parts $\boldsymbol{\Omega}' = \boldsymbol{\Omega}'_{\Omega} + \boldsymbol{\Omega}'_{P} + \boldsymbol{\Omega}'_{\nu}$, isolating rotations of the strain axis due to vorticity ($\boldsymbol{\Omega}'_{\Omega}$), off-diagonal pressure Hessian ($\boldsymbol{\Omega}'_{P}$), and viscous effects ($\boldsymbol{\Omega}'_{\nu}$).

Girimaji & Pope (1990) observe material line stretching rates in isotropic turbulence simulations that are significantly smaller than would be measured for an ideally persistent straining field. They attribute these smaller than expected stretching rates to the effects of vorticity and 'non-persistent straining'. ('Non-persistent straining' refers to misaligning effects due to the rotation of the principal strain axes.) To test this hypothesis it is necessary to isolate these effects from one another and compare their roles in reducing material line stretching rates. Girimaji & Pope investigate this by replacing the velocity gradient tensor in the material line evolution equation (2) with appropriately modified gradient tensors. Specifically, given a numerical velocity gradient tensor $\boldsymbol{A}(t)$ satisfying the simulated Navier–Stokes equation, (2) is modified to

$$\frac{\mathrm{d}}{\mathrm{d}t}\boldsymbol{l}(t) = \bar{\boldsymbol{A}}(0)\,\boldsymbol{l}(t) \tag{58}$$

to isolate the effects of vorticity, and into

$$\frac{\mathrm{d}}{\mathrm{d}t}\boldsymbol{l}(t) = \tfrac{1}{2}(\boldsymbol{A}(t) + \boldsymbol{A}^{\mathrm{T}}(t))\,\boldsymbol{l}(t) \tag{59}$$

to isolate the effects non-persistent straining. $\bar{\boldsymbol{A}}(0)$ in (58) is the one-time spatial-averaged gradient tensor. Girimaji & Pope conclude that both of these effects in isolation significantly limit alignment, and that this misaligning tendency will persist in the presence of both vorticity and non-persistent straining contributions.

It is evident from the expression for the strain rotation (57) that vorticity and the strain rotation are not in fact dynamically independent. Indeed, vorticity appears quadratically in the local strain rotation $\boldsymbol{\Omega}'_{\Omega}$ and in the non-local strain rotation $\boldsymbol{\Omega}'_{P}$. One can see that integrating the modified system (58) isolates only the balance between the vorticity rotating term $\boldsymbol{\Omega} \wedge \hat{\boldsymbol{\lambda}}$ and the stretching terms of the general

alignment equation (12). Also, (59) can be seen to isolate the balance between the entire strain rotation term $(\boldsymbol{\Omega}'_\Omega+\boldsymbol{\Omega}'_P+\boldsymbol{\Omega}'_\nu)\wedge\hat{\boldsymbol{\lambda}}$. We argue here that a more complete study of exactly how the turbulent straining field falls short of persistence should compare the relative importance of all of the relevant terms of the alignment equation (12). It would be difficult to isolate all of these terms in a manner similar to Girimaji & Pope. Instead the importance of these terms can be studied directly in the following way. Introducing the magnitude of the stretching terms of (12)

$$\mathscr{S} = \|\boldsymbol{S}\hat{\boldsymbol{\lambda}}\wedge\hat{\boldsymbol{\lambda}}\|, \tag{60}$$

we form the following dimensionless time-dependent quantities:

$$\left.\begin{aligned} \mathscr{Q}_\Omega(t) &= \|\boldsymbol{\Omega}\wedge\hat{\boldsymbol{\lambda}}\|/\mathscr{S}, \quad \mathscr{Q}'_\Omega(t) = \|\boldsymbol{\Omega}'_\Omega\wedge\hat{\boldsymbol{\lambda}}\|/\mathscr{S},\\ \mathscr{Q}'_P(t) &= \|\boldsymbol{\Omega}'_P\wedge\hat{\boldsymbol{\lambda}}\|/\mathscr{S}, \quad \mathscr{Q}'_\nu(t) = \|\boldsymbol{\Omega}'_\nu\wedge\hat{\boldsymbol{\lambda}}\|/\mathscr{S}. \end{aligned}\right\} \tag{61}$$

These quantities measure the instantaneous relative misaligning magnitudes of pure vorticity ($\mathscr{Q}_\Omega$), of vorticity via strain-axis rotation ($\mathscr{Q}'_\Omega$), of non-local off-diagonal pressure strain rotation ($\mathscr{Q}'_P$), and finally viscous strain rotation ($\mathscr{Q}'_\nu$). As a simple illustration we have measured such quantities along ABC flow trajectories and observe that the vorticity and pressure contributions to the strain-axis rotation play the dominant dynamic misaligning role (see §5 for details). It would be most revealing to study both time series and PDFs (in the spirit of Girimaji & Pope 1990 and the numerical section of this paper) for these quantities in turbulence simulations.

Vieillefosse (1982, 1984) is primarily concerned with studying the possibility of a finite-time vorticity singularity in the Euler equations. The presence or non-presence of this singularity is closely related to the persistence of the turbulent straining field. Vieillefosse analytically treats the gradients of the Euler equation ((55) and (56) without the viscous terms) by assuming a special form for the pressure field. Introducing the traceless symmetric velocity gradient $\boldsymbol{U} = \boldsymbol{S}-\frac{1}{3}\operatorname{trace}\boldsymbol{S}\boldsymbol{I}$, the tensor square of the vorticity $\boldsymbol{V} = \boldsymbol{\Omega}\otimes\boldsymbol{\Omega}$, and ignoring viscosity (55) and (56) become

$$\left.\begin{aligned} \frac{\mathrm{d}}{\mathrm{d}t}\boldsymbol{U} &= -\left(\boldsymbol{U}^2-\frac{\operatorname{trace}\boldsymbol{U}^2}{3}\boldsymbol{I}\right)-\left(\boldsymbol{V}-\frac{\operatorname{trace}\boldsymbol{V}}{3}\boldsymbol{I}\right)-\left(\boldsymbol{P}-\frac{\operatorname{trace}\boldsymbol{P}}{3}\boldsymbol{I}\right),\\ \frac{\mathrm{d}}{\mathrm{d}t}\boldsymbol{V} &= \boldsymbol{U}\boldsymbol{V}+\boldsymbol{V}\boldsymbol{U}. \end{aligned}\right\} \tag{62}$$

(Here $\boldsymbol{I}$ is the identity matrix.) The only possibility for closing this system of equations is to force the pressure second derivative to have the form

$$\boldsymbol{P} = \frac{\operatorname{trace}\boldsymbol{P}}{3}\boldsymbol{I} = \frac{\nabla^2 p}{3}\boldsymbol{I} = \frac{\sum_i \Omega_i^2 - s_i^2}{3}\boldsymbol{I}. \tag{63}$$

This form of the pressure second derivative is completely determined by the local shear and vorticity. In particular, the off-diagonal non-local terms are taken to be zero and the model, among other things, ignores the effects of pressure on the rotation of the strain axis. The physical meaning of these missing terms will be discussed below. Once this rather strong assumption is made, (62) can be greatly simplified and solved exactly. This analysis leads to the conclusion that vorticity asymptotically aligns with the intermediate strain direction $\hat{\boldsymbol{\xi}}_2$, that the intermediate shear s_2 is asymptotically positive and that both are singular. Both of these results

are consistent with several numerical simulations including those of Ashurst *et al.* (1987). Clearly Vieillefosse's model captures some of the observed features of vortex stretching in a turbulent fluid. We now turn to what is not captured in this model and to how one can made a new attack on this problem using a strain-basis alignment equation.

To illustrate what is physically missing from Vieillefosse's model we focus for the moment on the pressure contribution to the strain rotation. For an incompressible fluid the pressure field $p(\boldsymbol{x}, t)$ is related to the local shears and angular velocity through the Poisson equation

$$\nabla^2 p = -\operatorname{trace} \boldsymbol{A}^2 = \sum_i \Omega_i^2 - s_i^2 \equiv a, \tag{64}$$

which can be (formally) inverted to give the pressure second derivative (in Cartesian coordinates)

$$P_{ij}(\boldsymbol{x}, t) = \frac{1}{4\pi} \frac{\partial}{\partial x_i} \frac{\partial}{\partial x_j} \int \frac{\sum_i s_i^2(\boldsymbol{x}', t) - \Omega_i^2(\boldsymbol{x}', t)}{\|\boldsymbol{x} - \boldsymbol{x}'\|} \mathrm{d}^3 \boldsymbol{x}'. \tag{65}$$

Thus $\boldsymbol{\Omega}'_P$ depends quadratically on the vorticity and shears of nearby trajectories (including the very trajectory in question) and hence, if we assume that the integral (65) does not decay too fast, it is plausible that the non-local vorticity and shear contributions to the strain rotation are quite strong – possibly as strong as the local ones. This is likely to be the case close to or inside of regions of strong vorticity or shear (unless the shear and vorticity conspire to make $a(t)$ small). Indeed in Vieillefosse's model $a(t)$ diverges along the trajectory in question. Therefore the approximation given by (63) is likely to become inconsistent as this singularity is approached. However, at this time the precise role of non-local pressure contributions to vorticity stretching and alignment is not fully understood (She, Jackson & Orszag (1991)).

We suggest here that the strain-basis alignment formalism presented earlier may prove to be useful in understanding the observed vorticity alignment including a more general (than Vieillefosse) handling of the non-local effects of the pressure field. Equations (55) and (56) in the strain basis are

$$\left.\begin{aligned} \frac{\mathrm{d}}{\mathrm{d}t} s_j &= -s_j^2 + (\boldsymbol{\Omega}^2 - \Omega_j^2) - P_{jj} + \nu \nabla^2 s_j, \quad j = 1, 2, \\ \frac{\mathrm{d}}{\mathrm{d}t} \Omega_i &= s_i \Omega_i - ((\boldsymbol{\Omega}'_{\Omega} + \boldsymbol{\Omega}'_P) \wedge \boldsymbol{\Omega})_i + \nu \nabla^2 \Omega_i, \quad i = 1, 2, 3. \end{aligned}\right\} \tag{66}$$

One should note that the strain-axis rotating effects of viscosity (i.e. $\boldsymbol{\Omega}'_{\nu} \wedge \boldsymbol{\Omega}$ term) are not present since one can show that they are identically cancelled by terms arising from writing $\nabla^2 \boldsymbol{\Omega}$ in the strain basis. (However, the $\boldsymbol{\Omega}'_{\nu}$ terms are present in the evolution of material lines and this further supports the point made at the end of §2 that $\bar{\zeta}_{\text{vorticity}} > \bar{\zeta}_{\text{line}}$). In the limit of vanishing viscosity the strain and vorticity evolution equations can be written in the form

$$\frac{\mathrm{d}}{\mathrm{d}t} s_j = -s_j^2 + (\boldsymbol{\Omega}^2 - \Omega_j^2) - P_{jj}, \quad j = 1, 2, \tag{67}$$

$$\frac{\mathrm{d}}{\mathrm{d}t} \Omega_i = (s_i + \alpha_i) \Omega_i + \beta_i, \quad i = 1, 2, 3, \tag{68}$$

where $$\alpha_i = \sum_{j \neq i} \frac{\Omega_j^2}{s_j - s_i}, \quad \beta_i = \sum_{j \neq i} \frac{P_{ji}}{s_j - s_i} \Omega_j = -(\boldsymbol{\Omega}'_P \wedge \boldsymbol{\Omega})_i. \tag{69}$$

It is important to note that in the context of vortex stretching the 'rotation' of the strain axis due to vorticity acts as a nonlinear stretching term, not as a rotation. Thus, the signs and relative magnitudes of α_i (compared to the shears s_i) are of great dynamical significance. Since the stretching rates α_i are quadratic in vorticity this suggests that these 'rotation' terms are particularly important in regions where vorticity dominates shear (i.e. in the vortex structures observed in turbulence simulations (She *et al.* 1991)). Furthermore, using incompressibility and the ordering $s_1 \geqslant s_2 \geqslant s_3$ one can see that $\alpha_1(t) \leqslant 0$ and that $\alpha_3(t) \geqslant 0$ for all times t. It is evident that α_2 can be either positive or negative depending on the relative alignment of vorticity with the $\hat{\xi}_1$ and $\hat{\xi}_3$ directions. In either case, the nonlinear stretching terms *oppose* the production of vorticity – at least in the $\hat{\xi}_1$ and $\hat{\xi}_3$ directions. This opposition is particularly important in the $\hat{\xi}_1$ direction.

The above discussion of the nonlinear stretching rates α_i suggests the following Lagrangian description of vortex stretching dynamics. Suppose that at some time t the intermediate shear is approximately zero, i.e. $s_2(t) \approx 0$, and that the vorticity is weak, i.e. $\boldsymbol{\Omega}(t) \approx 0$. At this instant the nonlinear stretching rates α_i are small and vorticity will begin to stretch in the $\hat{\xi}_1$ direction. From (67) it follows that since $s_2 \approx 0$ the stretched $\hat{\xi}_1$ component of vorticity will cause s_2 to grow and become positive, resulting in an increase in Ω_2. As a consequence of this sequence of events α_1 will become large and negative and will quickly act to nullify the previous growth in Ω_1 (see (68)). Since s_2 is still small compared to s_1 the Ω_2 stretching will proceed for a *longer* time than the initial stretching of Ω_1 due to s_1. This relative long-time persistent alignment with $\hat{\xi}_2$ survives until Ω_2 itself becomes large at which point contraction of vorticity in the $\hat{\xi}_3$ direction becomes significant (due to the quadratic contribution of Ω_2 to the always positive nonlinear stretching rate α_3). The net result is that now α_2 becomes negative and large. This suppresses the previous stretching of the intermediate vorticity Ω_2. The alignment with the strong contracting direction causes a quick but not total destruction of the previous vorticity build-up. It should be emphasized that the relatively small magnitude of the intermediate shear s_2 implies that the vortex stretching in the intermediate direction is the most long-lived of the stretchings described in this scenario. This sequence of events is robustly observed in a variety of simulations that we have performed – even in the presence of random forms of the pressure terms – and is consistent with vortex stretching results in turbulence simulations (Ashurst *et al.* 1987; She *et al.* 1991). These results are discussed elsewhere.

5. Numerical results

The goal of the numerical simulations presented here is to study the extent to which strain is persistent in several examples of steady three-dimensional flows. As integrable flows should not lead to exponential stretching of material lines, we are primarily interested in studying flows with chaotic orbits. Nevertheless, regular orbits will be shown for comparison. We have chosen to study the Arnold–Beltrami–Childress (ABC) flows and the stretch–twist–fold (STF) flow of Bajer & Moffatt (1990). Although these two systems have a fluid mechanical origin and are important in dynamo theory they are obviously not 'turbulent' velocity fields. Nonetheless they provide interesting models exhibiting chaotic orbits (which can be

computed to a high degree of accuracy) and enable us to study in detail the phenomenology of the alignment equations. The ABC flows are a three-parameter family of flows given by

$$\left.\begin{aligned} u_x &= A\sin z + C\cos y, \\ u_y &= B\sin x + A\cos z, \quad 1 \geqslant A \geqslant B \geqslant C \geqslant 0, \\ u_z &= C\sin y + B\cos x. \end{aligned}\right\} \tag{70}$$

They satisfy the steady-state Euler equation, and for certain parameter values and initial conditions exhibit chaotic orbits. Following Dombre *et al.* (1986) we take $A = 1$, $B = 1/\sqrt{2}$, $C = 1/\sqrt{3}$ and use initial condition $\boldsymbol{x}_0 = (0,0,0)$ to generate a typical chaotic trajectory (nearby initial conditions are also used to show that measurements do not depend on which chaotic trajectory is chosen). We take $\boldsymbol{x}_0 = (1.25, 0, 0)$ (again using neighbours to test) to generate a typical regular orbit.

The STF flow are a two-parameter family of Stokes flows defined in the unit sphere $x^2+y^2+z^2 \leqslant 1$ with velocity field

$$\left.\begin{aligned} u_x &= \alpha z - 8xy, \\ u_y &= 11x^2 + 3y^2 + z^2 + \beta xz - 3, \quad \alpha, \beta \text{ real}, \\ u_z &= -\alpha x + 2yz - \beta xy. \end{aligned}\right\} \tag{71}$$

As in the numerical studies of Bajer & Moffatt we fix $\beta = 1$ and increase α from 0 to some appropriately large value (we use $\alpha = 5$). When the parameter $\alpha = 0$, orbits are periodic and lie on invariant surfaces. As the parameter α is increased from 0 orbits begin to jump randomly between surfaces which closely resemble the $\alpha = 0$ invariant surfaces (Bajer & Moffatt term this phenomenon 'super-adiabatic drift'). Eventually, for α values of approximately unity, orbits become chaotic and tend to fill the sphere ergodically. For large α orbits settle to a quasi-periodic behaviour. Regardless of the value of α, we pick the same initial condition $x_0 = y_0 = 0.25$, $z_0 = 0$ (other initial conditions give similar results and are not presented here).

Using the above flows to generate fluid-particle trajectories, simulations are performed as follows. We use the Burlisch–Stoer method (Press *et al.* 1986) to simultaneously integrate the evolution equations

$$\left.\begin{aligned} \frac{\mathrm{d}}{\mathrm{d}t}\boldsymbol{x} &= \boldsymbol{u}(\boldsymbol{x}, t), \quad \boldsymbol{x}(0) = \boldsymbol{x}_0, \\ \frac{\mathrm{d}}{\mathrm{d}t}\hat{\boldsymbol{l}} &= \boldsymbol{A}\hat{\boldsymbol{l}} - \langle \hat{\boldsymbol{l}}, \boldsymbol{A}\hat{\boldsymbol{l}} \rangle \hat{\boldsymbol{l}}, \quad \hat{\boldsymbol{l}}(0) = \hat{\boldsymbol{l}}_0. \end{aligned}\right\} \tag{72}$$

After choosing a random material line initial condition $\hat{\boldsymbol{l}}_0$ and integrating away transients, we record $\boldsymbol{x}(t), \hat{\boldsymbol{l}}(t)$, and the alignment-relevant quantities deriving from $\boldsymbol{x}(t)$ and $\hat{\boldsymbol{l}}(t)$. More precisely, the given velocity field $\boldsymbol{u}$ allows us to track the angular velocity $\boldsymbol{\Omega}(t)$, the strain tensor $\boldsymbol{S}(t)$ and strain tensor derivative $\dot{\boldsymbol{S}}(t)$ and, from these quantities, the eigenvalues $s_i(t)$, eigenvectors $\hat{\boldsymbol{\xi}}_i$, eigenvector rotation $\boldsymbol{\Omega}'(t)$, the cosines of the alignment angles $\hat{\boldsymbol{\lambda}}(t)$, and the exponential separation $\zeta_{\text{line}}(t)$. (Calculations for surface stretching and vortex stretching rates are not presented here.) For the numerical results presented below we have varied the initial conditions $\boldsymbol{x}_0$ and $\hat{\boldsymbol{l}}_0$ as well as the length of the sampled trajectory and the error tolerance of the

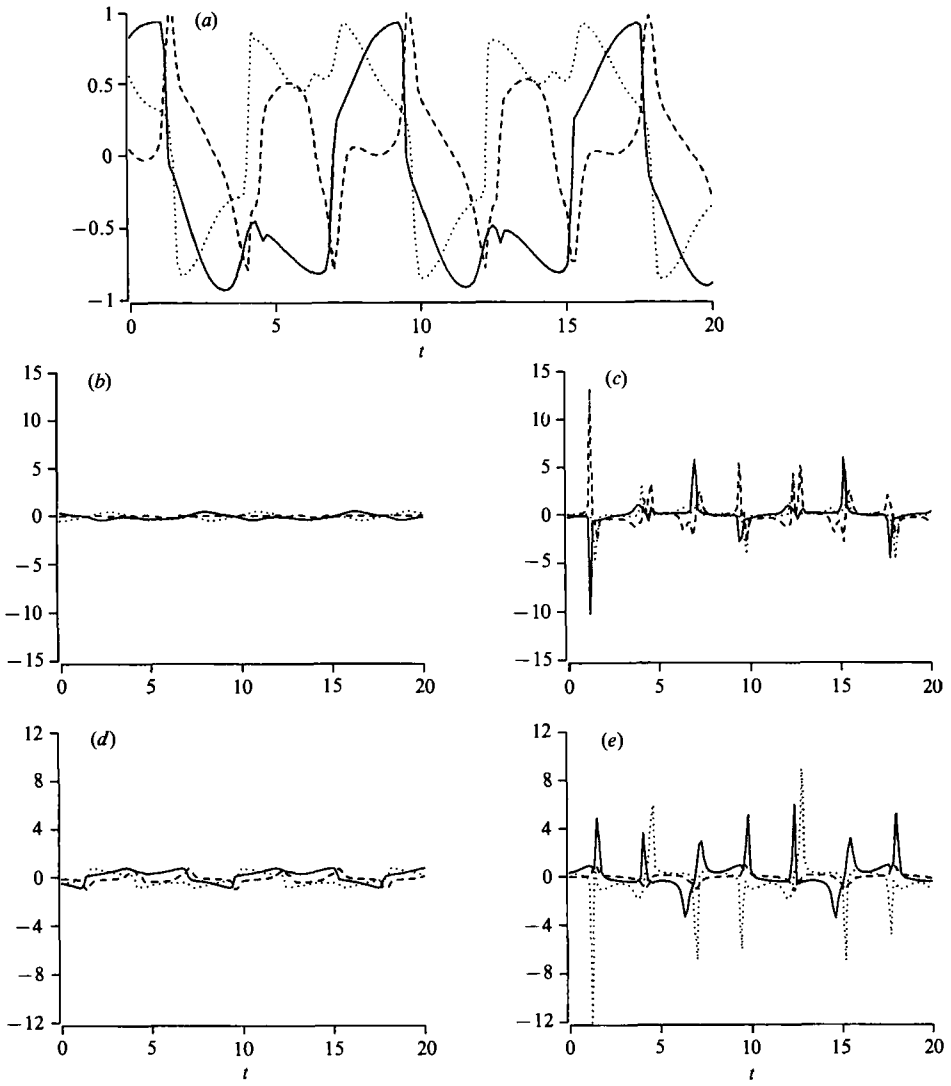

FIGURE 1. Time series for a single periodic trajectory of the ABC flows. The parameters values are $A = 1, B = 1/\sqrt{2}, C = 1/\sqrt{3}$; the initial condition is the point $x = 1.25, y = z = 0$. Time series for the following Lagrangian quantities are shown: (*a*) the components of the alignment vector $\lambda_1(t)$, $\lambda_2(t), \lambda_3(t)$; (*b*) the components of the alignment enhancing terms $\dot{\lambda}_1^+, \dot{\lambda}_2^+, \dot{\lambda}_3^+$; (*c*) the components of the alignment rotation terms $\dot{\lambda}_1^-, \dot{\lambda}_2^-, \dot{\lambda}_3^-$; (*d*, *e*) the three components of the angular velocity Ω_1, Ω_2, Ω_3 and eigenvector rotation $\Omega_1', \Omega_2', \Omega_3'$, respectively. Strain-basis components: ——, ξ_1; – – –, ξ_2; ....., ξ_3.

ODE integrator to verify that the results are numerically trustworthy. Eigenvalues and eigenvectors are found using a standard Jacobi rotation method. Care must be taken at each time step to maintain the correct choice of eigenvector signs. Recall that we have ordered the eigenvalues and required that $\det \boldsymbol{X} = +1$; these constraints must be preserved for all times. The only arbitrariness comes in the initial choice of eigenvector sign.

The data from the integrated trajectories are given here both as time series and in the form of probability distributions. The time series show us the short-time

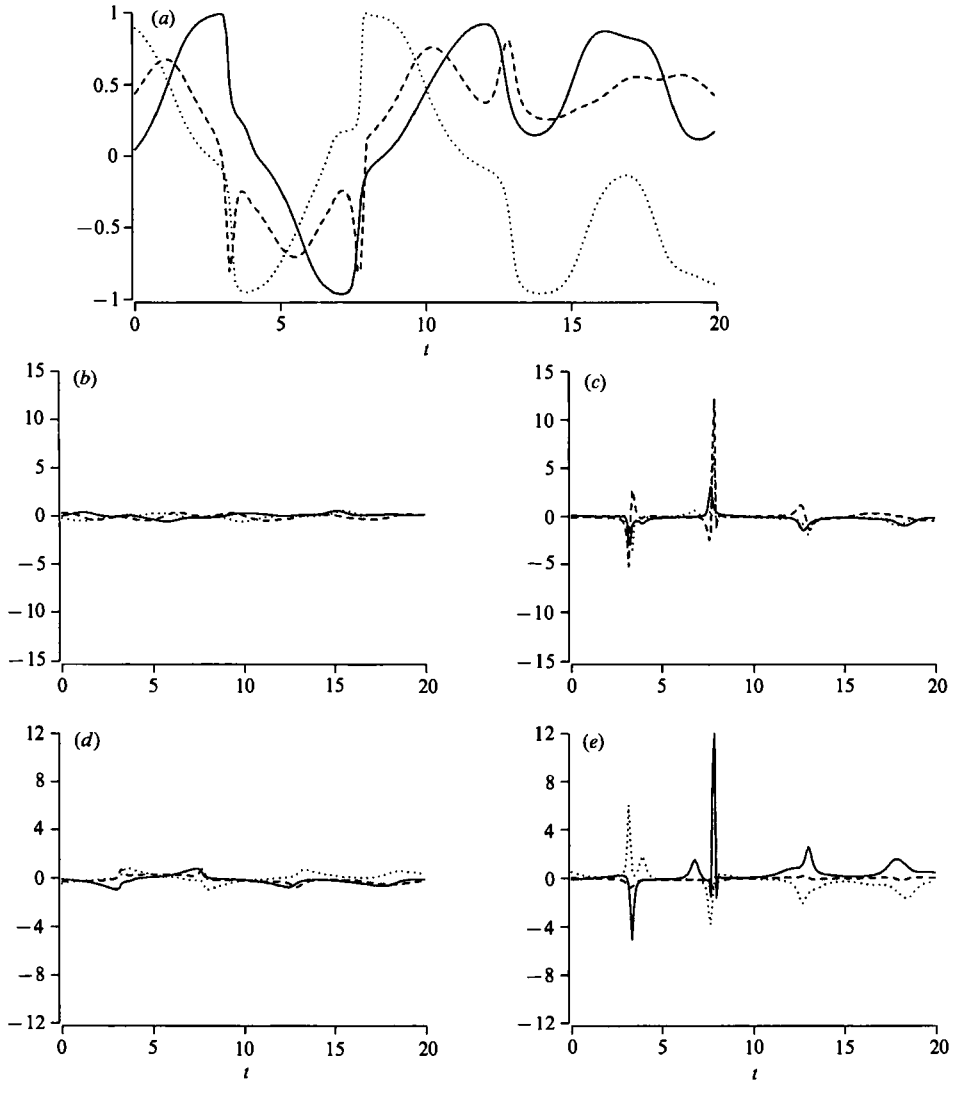

FIGURE 2. Time series for a single chaotic trajectory of the ABC flows. The parameters values are $A = 1, B = 1/\sqrt{2}, C = 1/\sqrt{3}$; the initial condition is the point $x = y = z = 0$. The quantities shown are as in figure 1.

dynamics of the alignment quantities. From this we can tell – at least for the flows we present here – which of the terms of the alignment equation play the dominant role. Specifically, we can isolate the effects of the 'alignment enhancing' terms

$$\frac{\mathrm{d}}{\mathrm{d}t}\hat{\boldsymbol{\lambda}}^{+}(t) = \begin{pmatrix} s_1 & 0 & 0 \\ 0 & s_2 & 0 \\ 0 & 0 & s_3 \end{pmatrix}\hat{\boldsymbol{\lambda}} - \zeta_{\mathrm{line}}\,\hat{\boldsymbol{\lambda}} \tag{73}$$

from the effects of the 'alignment rotating' term

$$\frac{\mathrm{d}}{\mathrm{d}t}\hat{\boldsymbol{\lambda}}^{-}(t) = (\boldsymbol{\Omega}(t) - \boldsymbol{\Omega}'(t)) \wedge \hat{\boldsymbol{\lambda}}(t). \tag{74}$$

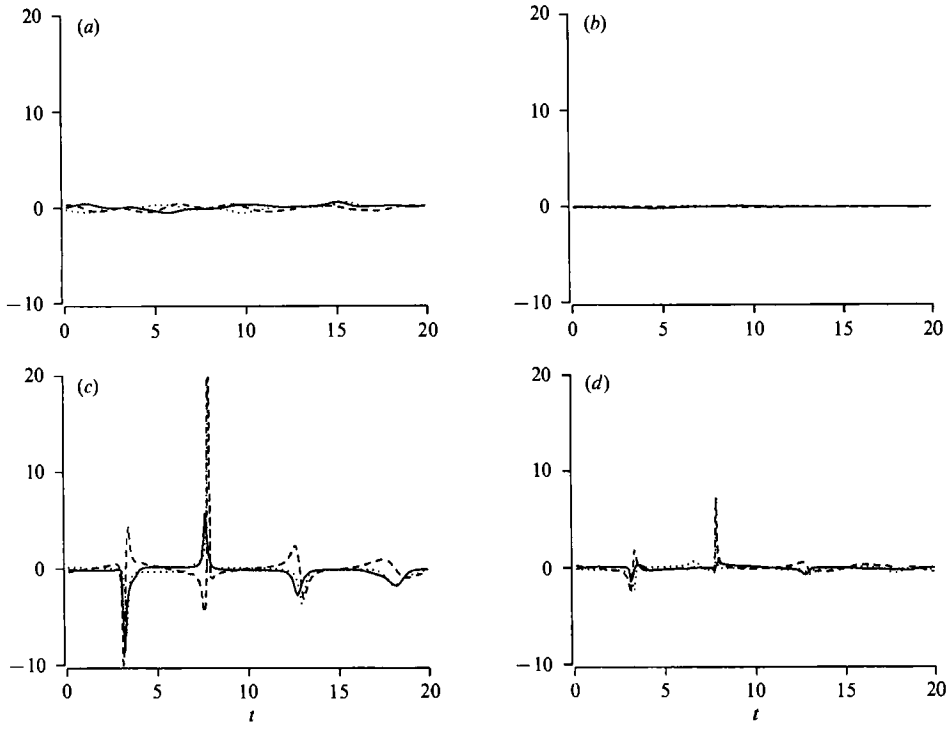

FIGURE 3. Time series for a single chaotic trajectory of the ABC flows showing the effects of non-local pressure. The parameters values are $A = 1, B = 1/\sqrt{2}, C = 1/\sqrt{3}$; the initial condition is the point $x = y = z = 0$. Time series for the following Lagrangian quantities are shown: (*a*) the components of the stretching term $(s_i - \zeta_{\text{line}})\lambda_i$; (*b*) the components of the rotation due to vorticity $\boldsymbol{\Omega} \wedge \hat{\boldsymbol{\lambda}}$; (*c*) the components of the strain rotation due to vorticity $\boldsymbol{\Omega}'_{\Omega} \wedge \hat{\boldsymbol{\lambda}}$; and (*d*) the components of the strain rotation due to pressure $\boldsymbol{\Omega}'_{P} \wedge \hat{\boldsymbol{\lambda}}$. Strain-basis components: ——, ξ_1; – – –, ξ_2; ·····, ξ_3.

Long-time features of the time series are encapsulated in probability distribution functions (PDFs). PDFs for several of the quantities we present are commonly measured in turbulence simulations (see Girimaji & Pope 1990, for example). PDFs for quantities such as the eigenvector rotation $\boldsymbol{\Omega}'$ are not traditionally studied and we believe that such studies should give valuable insight into material element and vorticity alignment issues for simulated turbulent flows.

The main conclusion from the simulations presented below is that strain is far from persistent for the flows we have considered. The mean line stretching rate for regular orbits is, of course, zero. However, even for chaotic ABC and STF flow trajectories we find that $\overline{\zeta}_{\text{line}} \approx \frac{1}{10}\overline{s}_1$, significantly less than that calculated by Girimaji & Pope (1990) using velocity fields derived from direct numerical simulation of the Navier–Stokes equation (Girimaji & Pope calculate $\overline{\zeta}_{\text{line}} \approx \frac{1}{3}\overline{s}_1$). Noting that $\overline{\zeta}_{\text{line}}/\overline{s}_1$ is bounded above by 1 and below by 0, we emphasize that the value of $\frac{1}{10}$ is indeed small.

Alignment time series for regular and chaotic ABC flow trajectories are shown in figures 1 and 2 respectively. Even in the short times displayed here both trajectories show poor alignment with $\hat{\boldsymbol{\xi}}_1$. For both trajectories it can be seen (compare figures 1*b* with 1*c*, and 2*b* with 2*c*) that the poor alignment is due to the action of the rotation term $\mathrm{d}/\mathrm{d}t\,\hat{\boldsymbol{\lambda}}^{-}(t)$. Furthermore, the rotation term is itself dominated by 'bursts' in the eigenvector rotation (compare figures 1*d* with 1*e*, and 2*d* with 2*e*). As $\boldsymbol{\Omega}'(t)$ becomes

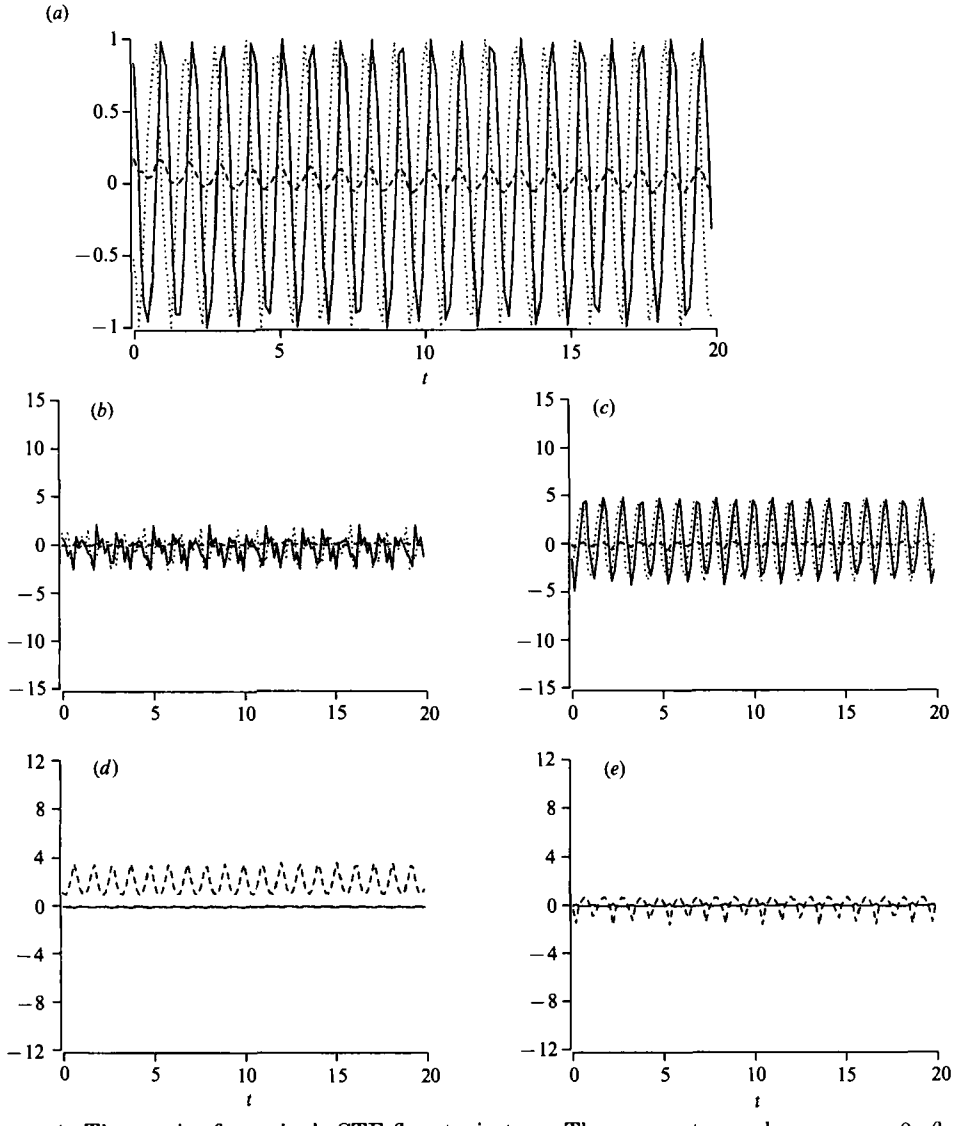

FIGURE 4. Time series for a single STF flow trajectory. The parameters values are $\alpha = 0$, $\beta = 1$; the initial condition is the point $x = y = 0.25$, $z = 0$. The quantities shown are as in figure 1.

large the strain axes jerk sharply and alignment is disrupted. For the regular orbit (figure 1) these disruptions occur significantly more frequently and with larger amplitude than for the chaotic orbit. The frequency and strength of these disruptions tend not to give the material line adequate time to align with $\hat{\boldsymbol{\xi}}_1$. The chaotic trajectory (figure 2) has more time to align with $\hat{\boldsymbol{\xi}}_1$ between disruptions. This explains, at least dynamically, how non-zero exponential line stretching is only achieved for the chaotic ABC flow trajectory. Figure 3 gives a simple illustration of the strain rotating effects of non-local pressure for the same chaotic ABC flow trajectory studied above. Material line rotation terms due to vorticity ($\boldsymbol{\Omega} \wedge \hat{\boldsymbol{\lambda}}$), vorticity strain-axis rotation ($\boldsymbol{\Omega}'_{\Omega} \wedge \hat{\boldsymbol{\lambda}}$), and pressure strain-axis rotation ($\boldsymbol{\Omega}'_{\mathrm{P}} \wedge \hat{\boldsymbol{\lambda}}$) are compared with the material line stretching terms. It is clear from figure 3 that the dominant rotation terms are due to $\boldsymbol{\Omega}'_{\Omega}$ and to a lesser degree to $\boldsymbol{\Omega}'_{P}$.

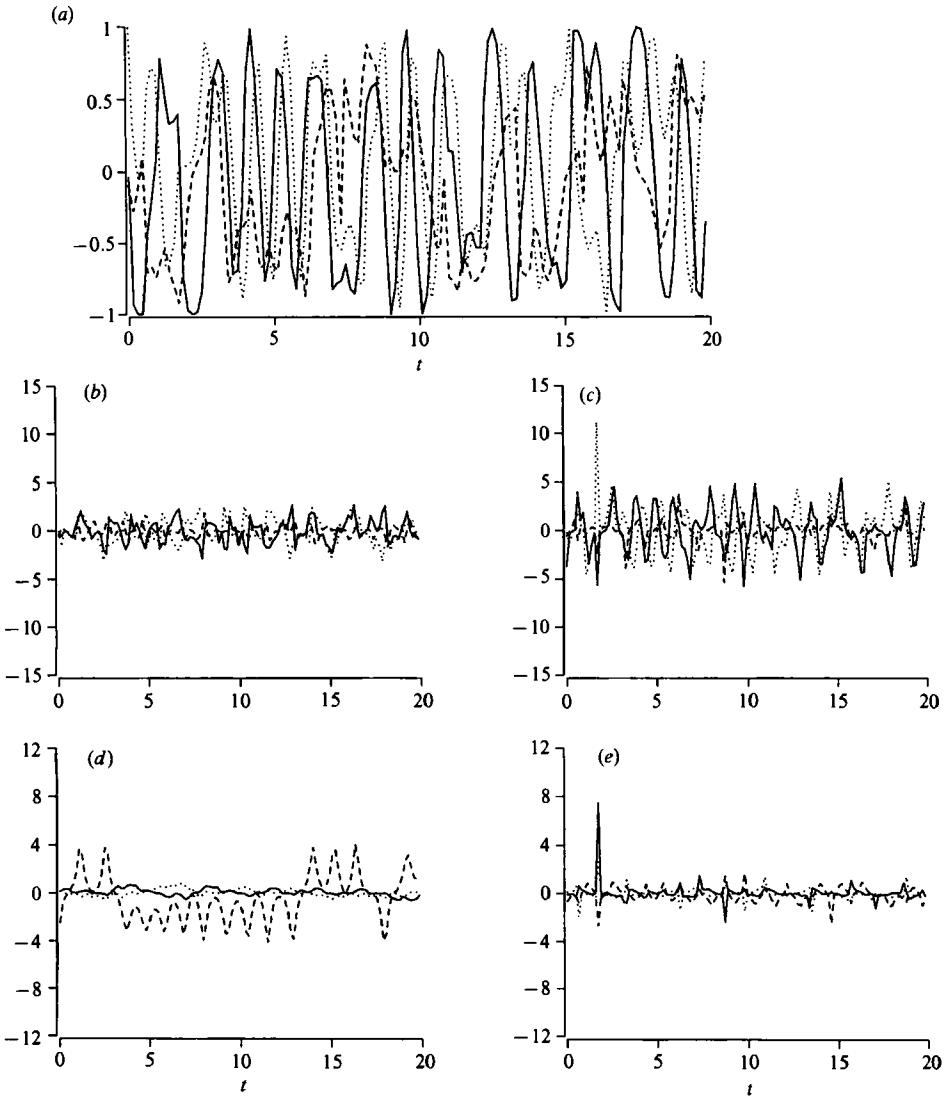

FIGURE 5. Time series for a single STF flow trajectory. The parameters values are $\alpha = 1$, $\beta = 1$; the initial condition is the point $x = y = 0.25$, $z = 0$. The quantities shown are as in figure 1.

Alignment time series for the STF flow with α values of 0 (periodic), 1 (chaotic), and 5 (quasi-periodic) are shown in figures 4, 5, and 6, respectively. Once again it can be seen that the dominant role is taken by the rotation terms of the alignment equation. However, for the STF flow trajectories pictured here both the eigenvector rotation and the angular velocity are important. It is difficult to see from these time series exactly how mean line stretchings of about zero (for $\alpha = 0, 5$ orbits) and about $\frac{1}{10}$ (for the $\alpha = 1$ orbit) are achieved. Insight into the alignment properties of these STF flow orbits will be found in the PDF studies presented below.

The sharp peaks in the eigenvector rotation are caused by approximate degeneracies of the eigenvalues (cf. (11)). There are two cases of approximate degeneracies: $s_1 \approx s_2$ (which makes Ω_3' large) and $s_2 \approx s_3$ (which makes Ω_1' large). In either case the near degeneracies in the numerical simulations are never near enough

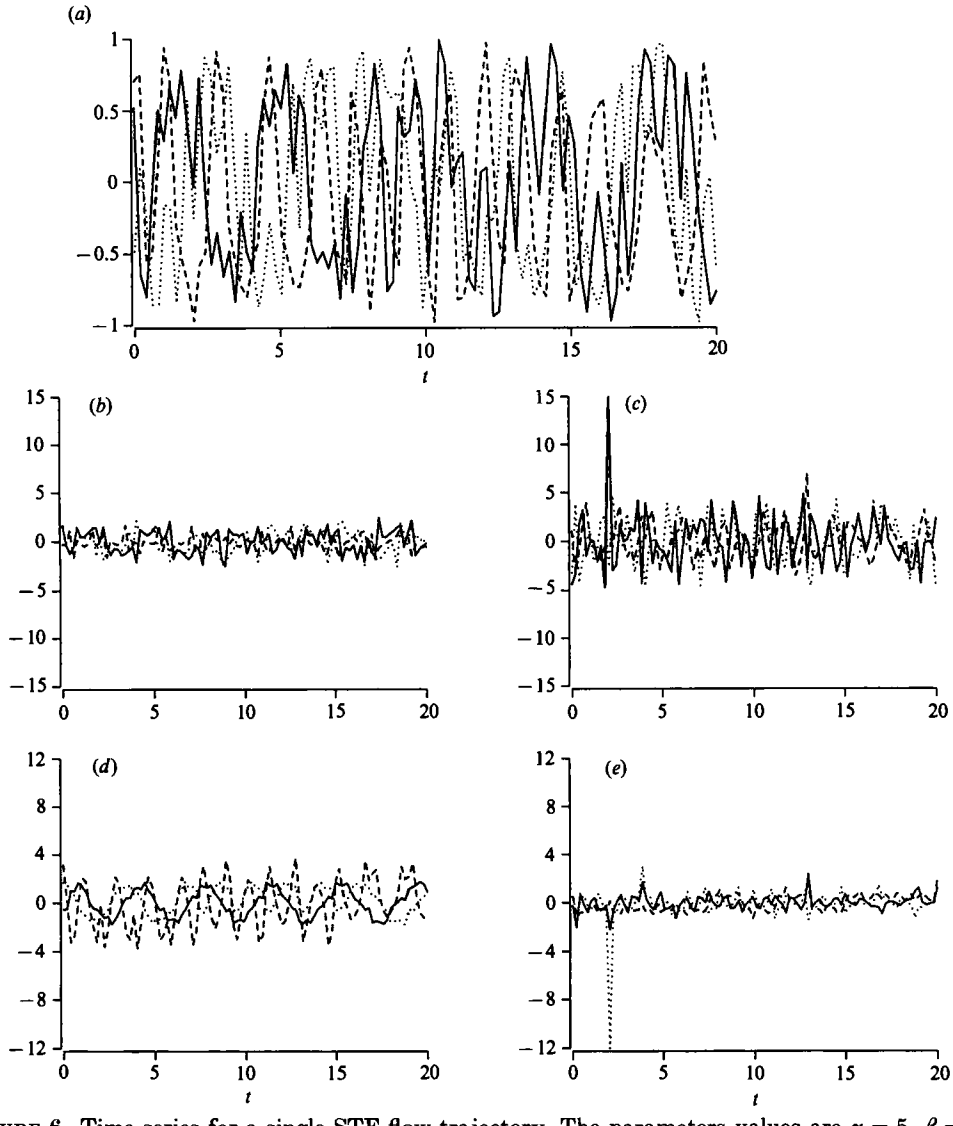

FIGURE 6. Time series for a single STF flow trajectory. The parameters values are $\alpha = 5$, $\beta = 1$; the initial condition is the point $x = y = 0.25$, $z = 0$. The quantities shown are as in figure 1.

to make any component of $\boldsymbol{\Omega}'$ larger than of order 100 inverse time units. Thus, we trust that our results are not sensitive to possible singularities in the denominator of (10). We believe that the frequency with which these two states of near degeneracy are reached plays a fundamental role in the general alignment problem.

The time series presented above only show alignment variables for short times. We introduce PDFs to obtain a sense of the long-time dynamics of alignment quantities. Specifically, figures 7–11 present PDFs corresponding to the trajectories of figures 1–5 for the following quantities: (*a*) the alignment cosines $\hat{\lambda}$, (*b*) the exponential line stretching, (*c*) the principal shears s_1, s_2, and s_3, (*d*) the Cartesian velocity u_x, u_y, and u_z, (*e*) the strain-base angular velocity $\Omega_1, \Omega_2, \Omega_3$, and, finally, (*f*) the eigenvector rotation $\Omega_1', \Omega_2', \Omega_3'$.

A striking feature of many of the PDFs is that they exhibit considerable

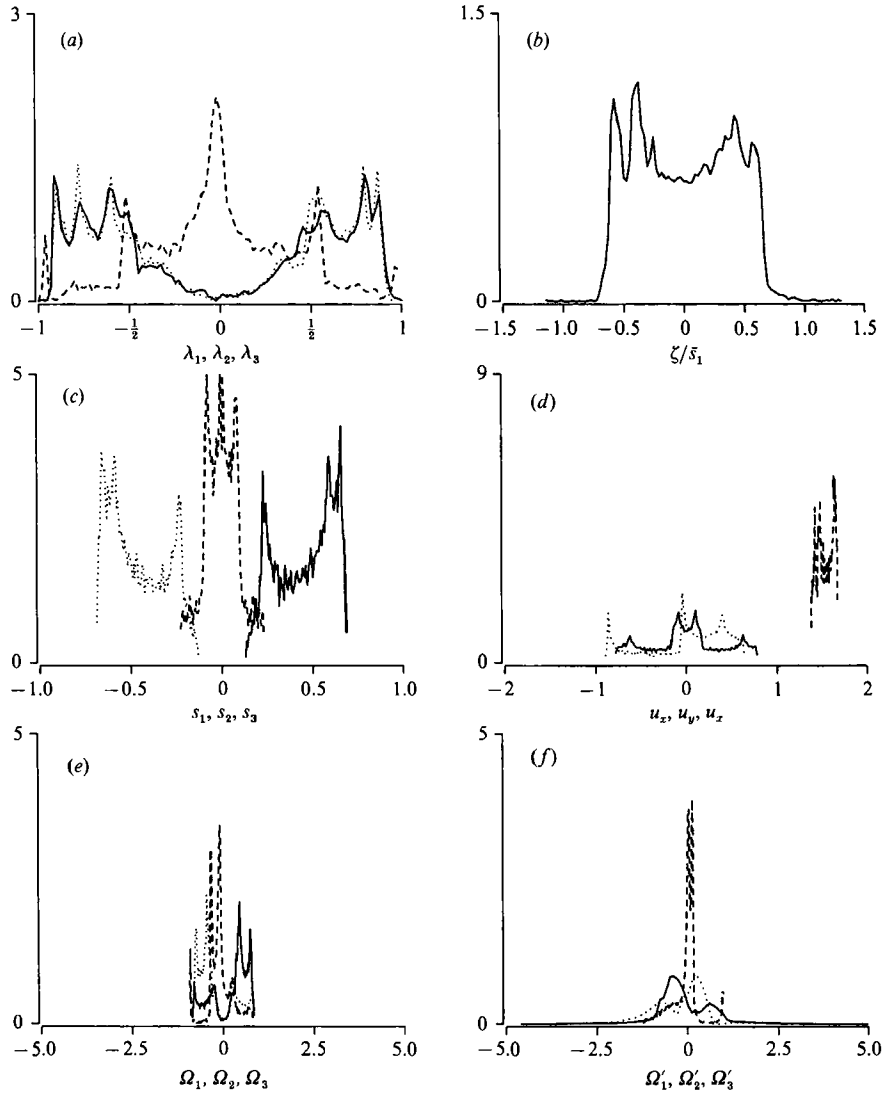

FIGURE 7. Probability distributions for a single periodic trajectory of the ABC flows. The parameters values are $A = 1$, $B = 1/\sqrt{2}$, $C = 1/\sqrt{3}$; the initial condition is the point $x = 1.25$, $y = z = 0$. PDFs for the following Lagrangian quantities are shown: (*a*) components of the alignment vector $\lambda_1(t), \lambda_2(t), \lambda_3(t)$; (*b*) the normalized exponential line separation $\zeta_{\text{line}}/\bar{s}_1$; (*c*) the shears s_1, s_2, s_3; (*d*) the Cartesian components of the velocity vector u_x, u_y, u_z; (*e*, *f*) the three components of the angular velocity $\Omega_1, \Omega_2, \Omega_3$ and eigenvector rotation $\Omega'_1, \Omega'_2, \Omega'_3$, respectively. Strain, Cartesian components: ——, ξ_1, x; – – –, ξ_2, y; ....., ξ_3, z.

symmetry. For example the eigenvalue PDFs are always (i.e. for both chaotic and regular orbits for both ABC and STF flows) nearly symmetric under the transformation

$$(s_1, s_2, s_3) \mapsto (-s_3, -s_2, -s_1) \tag{75}$$

(see figures 7*c*–11*c*). Quantities which depend on the eigenvectors $\hat{\xi}_i$, such as $\boldsymbol{\Omega}$, $\boldsymbol{\Omega}'$, and $\hat{\boldsymbol{\lambda}}$ are nearly symmetric under the transformation

$$(q_1, q_2, q_3) \mapsto (\sigma_3 q_3, \sigma_1 \sigma_3 q_2, \sigma_1 q_1), \quad \sigma_1, \sigma_3 = \pm 1, \quad q_i = \Omega_i, \Omega'_i, \lambda_i, \tag{76}$$

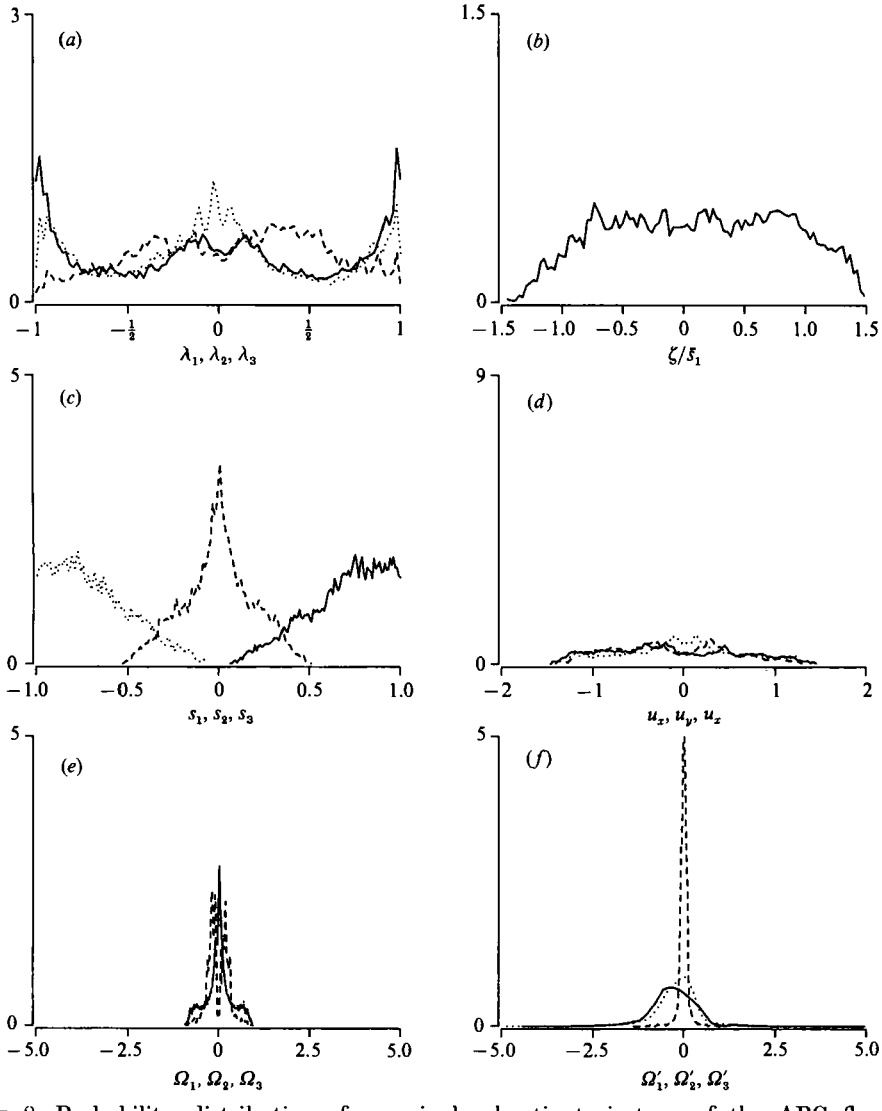

FIGURE 8. Probability distributions for a single chaotic trajectory of the ABC flows. The parameters values are $A = 1, B = 1/\sqrt{2}, C = 1/\sqrt{3}$; the initial condition is the point $x = y = z = 0$. The PDFs shown here as in figure 7.

but only for regular orbits (figures 7*a*, *e*, *f*, 9*a*, *e*, *f*, 11*a*, *e*, *f*). This symmetry is broken, albeit weakly, for chaotic orbits (figures 8*a*, *e*, *f* and 10*a*, *e*, *f*). Similarly, PDFs for ζ_{line} itself are completely symmetric for regular orbits (figures 7*b*, 9*b*, 11*b*), which is what one expects since these orbits should show no mean exponential stretching, and are only slightly skewed, with a mean of about $\frac{1}{10}$, for the chaotic orbits (figures 8*b* and 11*b*). At a heuristic level the very small values of $\bar{\zeta}_{\text{line}}$ an be argued to follow from the symmetric nature of the PDFs for the s_i (symmetric with respect to (75)) and the λ_i (symmetric with respect to (76)) since

$$\bar{\zeta}_{\text{line}} = \sum_i \overline{s_i \lambda_i^2} \approx \bar{s}_1(\bar{\lambda}_1^2 - \bar{\lambda}_3^2) \approx 0. \tag{77}$$

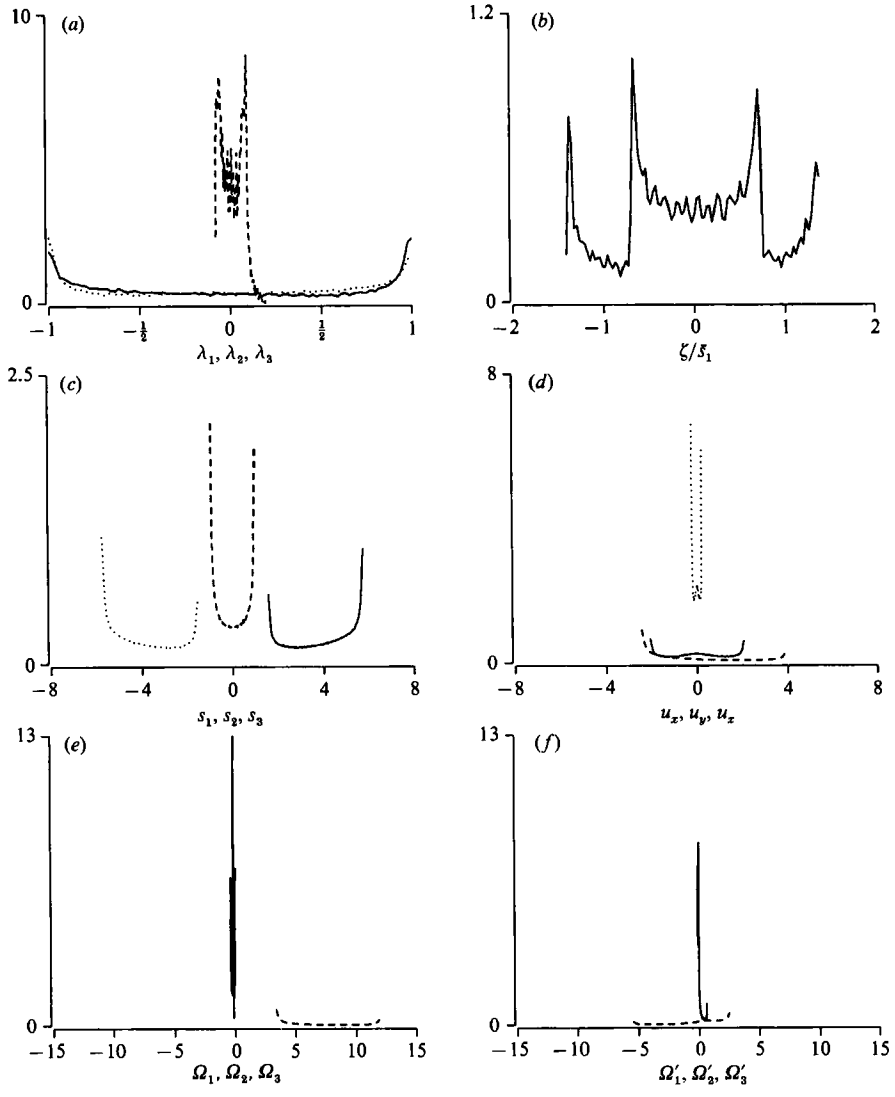

FIGURE 9. Probability distributions for a single STF flow trajectory. The parameters values are $\alpha = 0$, $\beta = 1$; the initial condition is the point $x = y = 0.25$, $z = 0$. The PDFs shown here are as in figure 7.

The decorrelation assumption, i.e. $\overline{s_i \lambda_i^2} \approx \bar{s}_i \bar{\lambda}_i^2$, needs to be justified although it does hold numerically to within 10% or so.

That the PDFs exhibit approximate symmetries follows from the fact that the Eulerian velocity fields themselves possess certain symmetries. In the case of the ABC flows these are three reflection symmetries (see Dombre *et al.* 1986 for details) and for the STF flow just one reflection symmetry. Although these symmetries are in the physical space of the dynamical system (i.e. in the Eulerian frame) the Lagrangian orbits, in the course of their time histories, sample these symmetries which then manifest themselves in the PDFs that we have computed. For quantities that do not depend on the eigenvectors $\hat{\xi}_i$, such as the velocity $\boldsymbol{u}$ and the eigenvalues s_i, the symmetry seen in the PDFs is easily explained in terms of the underlying

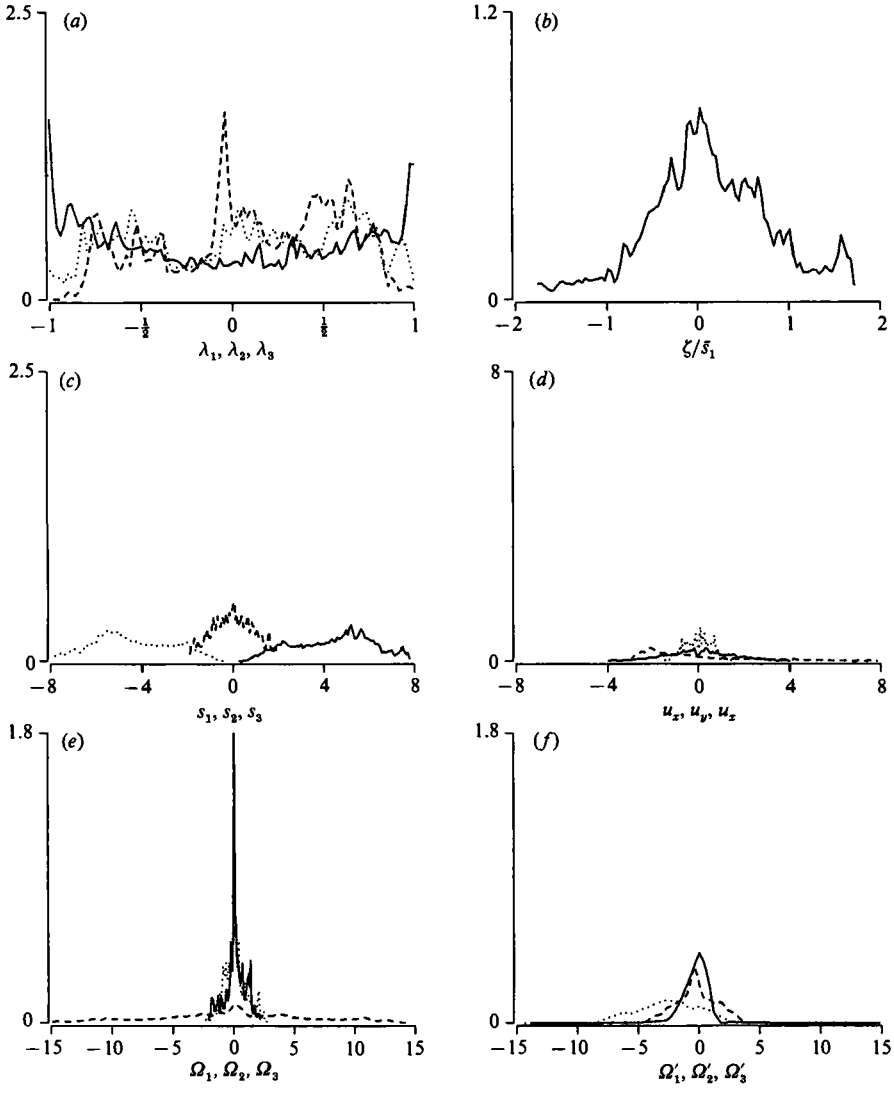

FIGURE 10. Probability distributions for a single STF flow trajectory. The parameters values are $\alpha = 1$, $\beta = 1$; the initial condition is the point $x = y = 0.25$, $z = 0$. The PDFs shown here are as in figure 7.

reflection symmetries of the flow field. For quantities that do depend on the eigenvectors, such as $\boldsymbol{\Omega}$, $\boldsymbol{\Omega}'$ and $\hat{\boldsymbol{\lambda}}$, the relationship between the symmetries in the PDFs and the Eulerian symmetries is more subtle since these quantities are influenced by additional equations of motion (specifically by the eigenvector evolution equation (10)) that may not possess the same symmetries as the flow field itself.

The symmetries that we see here and their consequences for the stretching and alignment kinematics are clearly specific to the particular flow fields studied and are unlikely to be relevant to real turbulence. Nonetheless it is important to realize that if a flow field has certain (discrete) symmetries these will influence measured dynamical quantities even if the sampled orbits are chaotic. Furthermore,

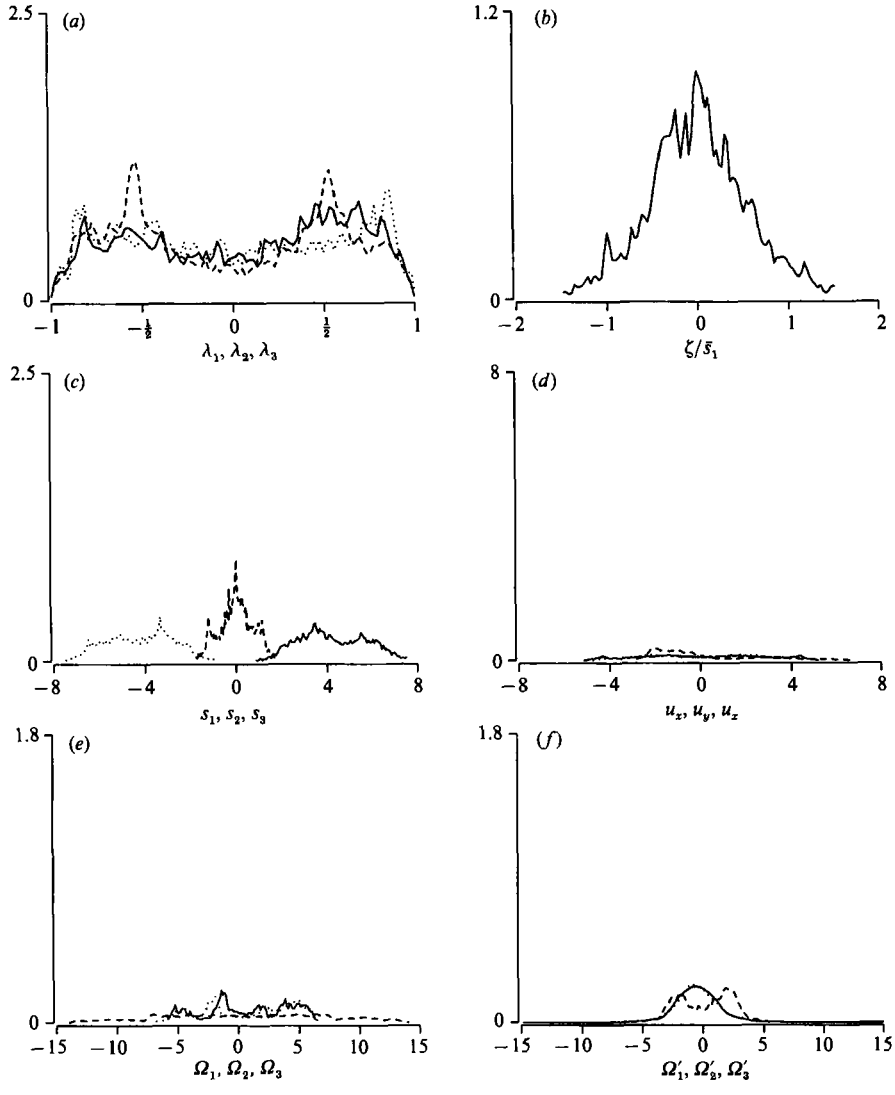

FIGURE 11. Probability distributions for a single STF flow trajectory. The parameters values are $\alpha = 5$, $\beta = 1$; the initial condition is the point $x = y = 0.25$, $z = 0$. The PDFs shown here are as in figure 7.

symmetries that are relevant to real fluid dynamical situations, such as time-reversal symmetry (Drummond & Münch 1990) or other symmetries that might be present, can clearly play an important role in the stretching and alignment properties of material elements.

6. Conclusion

By working in the rate-of-strain basis we have been able to provide a precise analysis of the stretching and alignment behaviour of material elements (equation (12)) and vorticity element (equation (19)). These results are purely kinematical (other than the assumption that vorticity satisfies the curl of the Euler equations (17)). These equations identify the complex role played by the competing effects of

vorticity and strain-basis rotation with the exact solutions for simple flow fields (§3) illustrating these effects. It is these effects that determine the extent of persistence/non-persistence of a given straining field. In addition the kinematics of (12) and (19) is sufficient to predict that mean vorticity stretching is greater than mean line stretching.

The formalism is applicable to any flow field, be it a fluid flow or that of some nonlinear dynamical system. However, in the particular case of the former, imposition of Navier–Stokes dynamics reveals special features of the stretching and alignment process. In particular the strain rotation vector (defined in (11)) is shown to be made of contributions from local vorticity, non-local pressure effects and viscous effects. It is the (quantifiable) contributions of these different effects that provides the detailed insight into the non-persistence of straining in fluid flows. Furthermore, the vorticity alignment equations can be analysed and shown to predict a loss of alignment with the strain axis with largest eigenvalue. This result provides a kinematic explanation of the observed vorticity alignment with the intermediate strain axis. An outstanding question is to understand the precise role of the non-local pressure terms in the alignment process.

There is obviously much scope for numerical study but here we have restricted ourselves to simple flow fields (both of interest in dynamo theory) to illustrate the basic phenomenology for chaotic particle paths. These results indicate a 'bursty' nature of strain-axis rotation, the surprisingly small value of mean local stretching and the role of symmetries in influencing stretching dynamics.

The authors thank the following individuals for helpful discussions: A. Bhattacharjee, C. C. Hegna, B. O'Shaughnessy, L. Polvani, D. Bessis, J. D. Fournier and H. K. Moffatt. This work is supported by AFOSR grant AFOSR-90-0284.

Appendix

Here we show that the eigenvector rotation $\boldsymbol{\Omega}'(t)$ for general two-dimensional particle paths is finite as the two principle shears become degenerate. In the following we will assume that the velocity gradients and their time derivatives are all finite at the time of degeneracy. Using the same notation as in §3, $\boldsymbol{\Omega}'(t)$ for these flows is given by (49):

$$\boldsymbol{\Omega}' = \frac{1}{2}\frac{\dot{a}b - a\dot{b}}{a^2+b^2}\hat{\boldsymbol{k}}. \tag{A 1}$$

The conditions that the shears be degenerate at a time $t = \tau$ is $a(\tau) = b(\tau) = 0$. Taking the limit of (A 1) as a and b tend to 0 one obtains from L'Hopital's rule

$$\Omega'(\tau) = \frac{1}{4}\frac{\ddot{a}\dot{b} - \dot{a}\ddot{b}}{\dot{a}^2+\dot{b}^2}. \tag{A 2}$$

Thus, $\Omega'(\tau)$ is finite unless $\dot{a}(\tau) = \dot{b}(\tau) = 0$ (recall, we have assumed that $\ddot{a}$ and $\ddot{b}$ are both finite). When the first time derivatives or higher time derivatives (or both) are zero at $t = \tau$ repeated applications of L'Hopital's rule implies that $\Omega'(\tau)$ is finite. The only possible failure of these repeated applications is the case where time derivatives of both a and b are zero to all orders – that is, that $a(t) = b(t) = 0$ for all $t \geqslant \tau$. In physical flows, of course, this cannot happen. Therefore, we conclude that $\boldsymbol{\Omega}'$ must be finite for any reasonable two-dimensional particle orbit.

REFERENCES

ASHURST, W. T., KERSTEIN, A. R., KERR, R. M. & GIBSON, C. H. 1987 Alignment of vorticity and scalar gradient with strain rate in simulated Navier–Stokes turbulence. *Phys. Fluids* **30**, 2343–2353.

BAJER, K. & MOFFATT, H. K. 1990 On a class of steady confined Stokes flows with chaotic streamlines. *J. Fluid Mech.* **212**, 337–363.

BATCHELOR, G. K. 1952 The effect of homogeneous turbulence on material lines and surfaces. *Proc. R. Soc. Lond.* A **213**, 349–366.

BATCHELOR, G. K. & TOWNSEND, A. A. 1956 Turbulent diffusion. In *Surveys in Mechanics* (ed. G. K. Batchelor & R. M. Davies), pp. 352–399. Cambridge University Press.

BETCHOV, R. 1956 An inequality concerning the production of vorticity in isotropic turbulence. *J. Fluid Mech.* **1**, 497–504.

COCKE, W. J. 1969 Turbulent hydrodynamic line stretching: consequences of isotropy. *Phys. Fluids* **12**, 2488–2492.

COCKE, W. J. 1971 Turbulent hydrodynamic line stretching: the random walk limit. *Phys. Fluids* **14**, 1624–1628.

DOMBRE, T., FRISCH, U., GREENE, J. M., HÉNON, M., MEHR, A. & SOWARD, A. M. 1986 Chaotic streamlines in the ABC flows. *J. Fluid Mech.* **167**, 353–391.

DRUMMOND, I. T. & MÜNCH, W. 1990 Turbulent stretching of line and surface elements. *J. Fluid Mech.* **215**, 45–59.

GIRIMAJI, S. S. & POPE, S. B. 1990 Material element deformation in isotropic turbulence. *J. Fluid Mech.* **220**, 427–458.

KRAICHNAN, R. H. 1970 Diffusion by a random velocity field. *Phys. Fluids* **13**, 22–31.

KRAICHNAN, R. H. 1974 Convection of a passive scalar by a quasi-uniform random straining field. *J. Fluid Mech.* **64**, 737–762.

MAJDA, A. J. 1991 Vorticity, turbulence, and acoustics in fluid flow. *SIAM Rev.* **33**, 349–388.

MONIN, A. M. & YAGLOM, I. 1975 *Statistical Fluid Mechanics*, vol. 2. MIT Press.

ORSZAG, S. A. 1970 Comments on 'Turbulent hydrodynamic line stretching: consequences of isotropy'. *Phys. Fluids* **13**, 2203–2204.

PRESS, W. H., FLANNERY, B. P., TEUKOLSKY, S. A. & VETTERLING, W. T. 1986 *Numerical Recipes*. Cambridge University Press.

SHE, Z.-S., JACKSON, E. & ORSZAG, S. A. 1991 Structure and dynamics of homogeneous turbulence: models and simulations. *Proc. R. Soc. Lond.* A **434**, 101–124.

TABOR, M. & GENNES, P. G. DE 1986 A cascade theory of drag reduction. *Europhys. Lett.* **2**, 519–522.

TOWNSEND, A. A. 1951 The diffusion of heat spots in isotropic turbulence. *Proc. R. Soc. Lond.* A **209**, 418–430.

VIEILLEFOSSE, P. 1982 Local interaction between vorticity and shear in a perfect incompressible fluid. *J. Phys. Paris* **43**, 837–842.

VIEILLEFOSSE, P. 1984 Internal motion of small element of fluid in an inviscid flow. *Physica* **125A**, 150.